# AMBRA1 promotes apoptosis induced by dsRNA and virus through interacting with and stabilizing MAVS

Yuxia Lin[1,2, #], Changbai Huang[1,2, #], Huixin Gao[1,2], Xiaobo Li[1,2], Quanshi Lin[1,2], Shili Zhou[1,2], Zhiting Huo[1,2], Yanxia Huang[1,2], Chao Liu[1,3,*], and Ping Zhang[1,2,*]

[1]Key Laboratory of Tropical Diseases Control (Sun Yat-sen University), Ministry of Education, Guangzhou 510080, China;

[2]Department of Immunology, Zhongshan School of Medicine, Sun Yat-sen University, Guangzhou 510080, China;

[3] Department of Microbiology, Zhongshan School of Medicine, Sun Yat-sen University, Guangzhou 510080, China

[#]These authors contributed equally to this work.

∗To whom correspondence should be addressed:

Ping Zhang, zhangp36@mail.sysu.edu.cn; Chao Liu, liuchao9@mail.sysu.edu.cn

## SUMMARY STATEMENT

We identified AMBRA1 as a new regulator of apoptosis induced by dsRNA or viral infection, and uncovered its role in interacting with and stabilizing a key adaptor (MAVS) in the apoptosis pathway.

## ABSTRACT

Apoptosis is an important cellular response to viral infection. In current study, we identified activating molecule in Beclin1-regulated autophagy protein 1 (AMBRA1) as a positive regulator of apoptosis triggered by dsRNA. Depletion of AMBRA1 by gene editing significantly reduced dsRNA-induced apoptosis, which was largely restored by *trans*-complementation of AMBRA1. Mechanistically, AMBRA1 interacts with mitochondrial antiviral-signaling protein (MAVS), a key mitochondrial adaptor in the apoptosis pathway induced by dsRNA and viral infection. Further Co-IP analysis demonstrated that the mitochondrial localization of MAVS was essential for their interaction. The impact of AMBRA1 on dsRNA-induced apoptosis relied on the presence of MAVS and caspase-8. AMBRA1 was involved in the stabilization of MAVS through preventing its proteasomal degradation induced by dsRNA. Consistently, AMBRA1 upregulated the apoptosis induced by Semliki Forest virus infection. Taken together, our work illustrated a role of AMBRA1 in the virus-induced apoptosis through interacting with and stabilizing MAVS.

**KEY WORDS:** apoptosis; virus; dsRNA; AMBRA1; MAVS

## INTRODUCTION

In response to viral infection, cell rapidly elicits multiple signaling pathways to mount different responses, including formation of stress granules, protein translation inhibition (McCormick and Khaperskyy, 2017), endoplasmic reticulum (ER) stress, unfolded protein response (UPR), autophagy (Chiramel et al., 2013), innate immunity (Takeuchi and Akira, 2009), and programmed cell death

(PCD) (Imre, 2020), etc. Among these responses, autophagy is a highly conserved pathway that maintains cellular homeostasis by removal of damaged or excess cellular components, thereby achieving cell survival. The autophagy pathway activated by virus may play either an antiviral or proviral role (Chiramel et al., 2013; Jordan and Randall, 2012). Programmed cell death (PCD) includes apoptosis, necroptosis, and pyroptosis (Imre, 2020; Nagata and Tanaka, 2017). Apoptosis is the most extensively studied cell death in the context of viral infection. Apoptosis occurs through two distinct pathways, the caspase 8-dependent extrinsic pathway initiated by death receptors of TNF family, and the caspase 9-dependent intrinsic pathway mediated by mitochondrial BCL-2 family members (Nagata and Tanaka, 2017). Necroptosis is a type of programmed necrosis mediated by receptor-interacting protein kinase (RIPKs) and its substrate mixed lineage kinase domain-like protein (MLKL) (Pasparakis and Vandenabeele, 2015). Pyroptosis is another type of programmed necrosis regulated by activated caspases, which cleave and activate substrates (IL-1β, IL-18, and gasdermin D). The N-terminal of gasdermin D forms holes in the plasma membrane, leading to pyroptotic cell death (Sanjo et al., 2019; Shi et al., 2015).

In terms of viral infection, a variety of factors are responsible for triggering cell death pathways, such as viral proteins, viral genomic nucleotides, and double-stranded RNA (dsRNA) that is a common byproduct of viral replication (Son et al., 2015). To date, a few cellular proteins have been reported to participate in the cell death triggered by viral infection. These proteins are mainly involved in innate immune pathway, including pattern recognition receptors (PRRs) like melanoma differentiation-associated gene 5 (MDA5), retinoic acid inducible gene I (RIG-I) and toll like receptor 3 (TLR3) (Amarante-Mendes et al., 2018), mitochondrial antiviral-signaling protein (MAVS, also known as IPS-1/VISA/Cardif) (Kawai et al., 2005), transcriptional factors like interferon

regulatory factor 3 (IRF3) (Chattopadhyay and Sen, 2017), and IFN stimulated genes (ISGs), such as dsRNA activated protein kinase (PKR) (Barber, 2005), 2'-5' oligoadenylate synthetase (OAS) and ribonuclease L (RNaseL) (Castelli et al., 1997; Chawla-Sarkar et al., 2003). To identify more regulators of cell death, we carried out a genome-wide CRISPR/Cas9-based screen utilizing poly(I:C), a synthetic dsRNA as death stimulator. We found a new gene, *AMBRA1* that encodes activating molecule in Beclin1-regulated autophagy protein 1 (AMBRA1) (Fimia et al., 2007), was among the top hits (data not shown).

AMBRA1 is highly conserved in vertebrates, and promotes the autophagy either by forming a complex with Beclin1 and Vps34 and then favoring the formation of autophagosomes (Di Bartolomeo et al., 2010; Fimia et al., 2011; Fimia et al., 2007), or by acting as an E3 ligase to ubiquitinate Beclin1 and finally promoting Beclin1-mediated Vps34 activity (Xia et al., 2013). Apart from autophagy, AMBRA1 positively or negatively regulates the apoptosis, depending on physiological and pathological conditions. The C-terminal part of AMBRA1 binds an anti-apoptotic protein BCL2 and inhibits its function, thus contributing to the onset of apoptosis induced by staurosporine (STS) (Strappazzon et al., 2016). In contrast, functional deficiency of AMBRA1 causes severe apoptosis in mouse embryos (Fimia et al., 2007) and downregulation of AMBRA1 sensitizes cells to apoptotic stimuli, like STS and etoposide (Pagliarini et al., 2012), implying that AMBRA1 also has an inhibitory effect on apoptosis. Whether AMBRA1 plays a pro-apoptosis or an anti-apoptosis effect is probably directed by its control of the conversion between autophagy and apoptosis. For an example, a pivotal role of AMBRA1 in positively regulating autophagy is often associated with its anti-apoptosis function (Gu et al., 2014; Li et al., 2016; Liu et al., 2019; Sun et al., 2018; Sun et al., 2019). Although AMBRA1 has been shown to regulate the apoptosis under various

physiological circumstances, the underlying mechanisms have been rarely investigated. Particularly, whether AMBRA1 acts in the virus-induced cell death has not been investigated.

In this study, we examined role of AMBRA1 in cell death induced by dsRNA or Semliki Forest virus (SFV) infection. We found that AMBRA1 confers a pro-apoptotic activity. In addition, our work illustrated the underlying mechanism by which AMBRA1 interacts with MAVS and prevents its proteasomal degradation. Finally, we demonstrated that the pro-apoptotic effect of AMRBA1 relies on the presence of MAVS.

## RESULTS

### AMBRA1 is involved in the dsRNA-induced cell death

To validate the CRISPR/Cas9 screen data showing AMBRA1 may have a potential function in the dsRNA-induced cell death, we utilized the CRISPR/Cas9 gene editing technique to generate AMBRA1 knockout (KO) cells. SgRNA against *AMBRA1* gene was selected from the pooled library used for CRISPR/Cas9-based screen (Fig. 1A). Two independent AMBRA1$^{KO}$ cell clones were isolated and designated as AMBRA1$^{KO}$-#1 and AMBRA1$^{KO}$-#2. The disruption of *AMBRA1* gene was confirmed by genomic DNA sequencing. One or more nucleotides were deleted in two AMBRA1$^{KO}$ cell clones (Fig. 1B), indicative of effective disruption of *AMBRA1* gene. In our study, the endogenous AMBRA1 in A549 cells could not be directly detected by anti-AMBRA1 antibodies from two different companies, possibly due to their short half-life as previously reported (Pagliarini et al., 2012). Then, we conducted a co-IP assay to enrich endogenous AMBRA1 protein, followed by western blot. As shown in Fig. 1C, AMBRA1 protein was readily detected in the control cells, but not in two AMBRA1$^{KO}$ cell clones, confirming the disruption of *AMBRA1* gene. In addition,

qRT-PCR data showed that the mRNA levels of *AMBRA1* in both AMBRA1$^{KO}$ cell clones were remarkably decreased (~90%, Fig. 1D). To rule out potential off-target effect of *AMBRA1*-specific sgRNA, we introduced *AMBRA1* gene back to #2 knockout cell clone by lentivirus-mediated transduction. The AMBRA1-complemented cells, designated as AMBRA1$^{RES}$, were sorted by flow cytometry. The qRT-PCR data revealed that the mRNA levels of *AMBRA1* were successfully restored in AMBRA1$^{RES}$ cells (Fig. 1D).

To examine role of AMBRA1 in the dsRNA-induced cell death, we compared the cell viabilities of AMBRA1 sufficient and deficient cells. We first optimized the dose of poly(I:C) transfected into cells. The control and AMBRA1$^{KO}$ cells were transfected with different doses of poly(I:C) ( 0.5, 1, and 1.5 μg/ml), and at 24 h post-transfection, the cell viabilities were measured. Control cells underwent cell death upon poly(I:C) treatment，and the extents of cell death were correlated with the doses of poly(I:C). The cell viabilities of AMBRA1$^{KO}$ were about 1.4-, 2-, and 1.8-fold higher than control cells at 0.5, 1, and 1.5 μg/ml poly(I:C) respectively (Fig. S1A). Therefore, 1 μg/ml of poly(I:C) were used in the following assays unless indicated. At 24 h post-transfection, the viability of control cells was ~10% (black columns, Fig. 1E), while the viabilities of two knockout cell clones were ~30% (Fig. 1E). As expected, complementation of AMBRA1 resulted in the cell viability to a comparable level as control cells (Fig. 1E). Under microscopy, characterizations of cell death, including membrane blebbing and cell shrinkage were observed in poly(I:C)-treated control and AMBRA1$^{RES}$ cells, while the degree of cell death in the AMBRA1$^{KO}$ cells was significantly reduced (Fig. 1F).

In addition, we generated two AMBRA1$^{KO}$ cell clones in HeLa cells and validated the successful editing by genomic DNA sequencing (Fig. S1B) and qRT-PCR data (Fig. S1C). In HeLa cells, depletion of AMBRA1 also led to a reduction of cell death induced by dsRNA (Fig. S1D and S1E). Altogether, these observations indicated that AMBRA1 positively regulates the dsRNA-induced cell death.

**AMBRA1 is involved in the apoptosis induced by dsRNA**

As dsRNA can induce three types of programmed cell death, including apoptosis (Zhao et al., 2012), necroptosis (Takaki et al., 2017; Yu et al., 2017), and pyroptosis (Sanjo et al., 2019), we explored which type of cell death AMBRA1 mediates. First, we evaluated whether the cell death is affected by inhibitors of apoptosis or RIPK1, a key mediator of necroptosis. The control and AMBRA1$^{KO}$ cells were transfected with poly(I:C) in the presence of vehicle (DMSO), an apoptosis inhibitor z-VAD(OMe)-FMK (zVAD), or a RIPK1 inhibitor Necrostatin-1 (Necro-1) (Gao et al., 2019). Cell viabilities were measured by MTT assay at 24 h post-transfection. In the control cells, zVAD treatment resulted in a dramatic increase of cell viability, reaching a similar level as AMBRA1$^{KO}$ cells (Fig. S2A), implying that AMBRA1 is involved in the apoptosis. In contrast, the cell viabilities of control or AMBRA1$^{KO}$ cells were not altered by Necro-1 treatment, indicating an exception of RIPK1-mediated necroptosis. (Wang et al., 2019). To further probe if RIPK1-independent necroptosis and pyroptosis occur in poly(I:C)-triggered A549 cells, we utilized necrosulfonamide (NSA), an inhibitor that blocks both necroptosis (Sun et al., 2012) and pyroptosis (Rathkey et al., 2018). A549 cells were stimulated with poly(I:C) in the presence of vehicle (DMSO) and different concentrations of NSA. The NSA treatment alone did not alter the cell viabilities (Fig.

S2B), suggesting that necroptosis and pyroptosis are not the main types of cell death in poly(I:C)-stimulated A549 cells.

To confirm that AMBRA1 regulates the poly(I:C)-induced apoptosis, we compared the apoptosis extents by western blot, immunofluorescence microscopy, and flow cytometry. Levels of caspase-3, an executor caspase of apoptosis, cleaved caspase-3 (c-caspase-3), and poly(ADP-ribose) polymerase (PARP), an apoptosis indicator, were detected by western blot. The ratio of c-caspase-3/caspase-3 in the AMBRA1$^{KO}$ cells was decreased compared to the control or AMBRA1$^{RES}$ cells at 9 h and 12 h post-transfection respectively (Fig. 2A). Likewise, the cleavage of PARP in the AMBRA1$^{KO}$ cells was decreased compared to the control or AMBRA1$^{RES}$ cells (Fig. 2A). Flow cytometry analysis showed that the percentage of apoptotic cells was significantly reduced in AMBRA1$^{KO}$ cells (around 41%) compared to the control cells (around 60%) and AMBRA1$^{RES}$ cells (around 68%) (Fig. 2B and 2C). Finally, we monitored the extent of cell karyopyknosis, another indicator of apoptosis, by immunofluorescence microscopy. In the mock-treated cells, the nuclei were intact, while the nuclear condensation was clearly visualized in poly(I:C)-treated cells (Fig. 2D). The percentage of cells with nuclear condensation was lower in the AMBRA1$^{KO}$ cells (about 22%) compared to the control (about 50%) and AMBRA1$^{RES}$ cells (about 48%). Similarly, in HeLa cells, the cleavage of PARP and karyopyknosis was remarkably decreased in the AMBRA1$^{KO}$ cells compared to the control cells (Fig. S2C and S2D). Collectively, our results demonstrated that AMBRA1 promotes the dsRNA-induced apoptosis.

**AMBRA1 interacts with MAVS**

Caspases play a vital role in the initiation and execution of apoptosis (Creagh et al., 2003). To distinguish role of caspase-8 and caspase-9, two key initiator caspases for extrinsic and intrinsic pathway respectively, in the poly(I:C)-induced apoptosis (Budihardjo et al., 1999; Van Opdenbosch and Lamkanfi, 2019), we utilized an RNA interference (RNAi) strategy. A549 cells were transfected with a negative control siRNA (siNC), *caspase-8*-specific siRNA (si-cas8), or *caspase-9*-specific siRNA (si-cas9) for 48 h, followed by poly(I:C) stimulation. At 9 h post-transfection of poly(I:C), the cells were harvested for western blot. The caspase-8 or caspase-9 protein levels in si-cas8-transfected or si-cas9-transfected cells were significantly lower than those in the siNC-transfected cells (Fig. 3A), indicating that knockdown of caspase-8 or caspase-9 was effective. The ratio of c-caspase-3/caspase-3 and the cleavage extents of PARP in mock-treated (lane 2, Fig. 3A) and siNC-treated cells (lane 4, Fig. 3A) were comparable. Knockdown of caspase-8 (lane 6, Fig. 3A), but not caspase-9 (lane 8, Fig. 3A), dramatically decreased the ratio of c-caspase-3/caspase-3 and the cleavage of PARP compared to that in mock-treated (lane 2, Fig. 3A) or siNC-treated cells (lane 4, Fig. 3A). Similarly, significant reductions of caspase-3 cleavage and PARP cleavage were also observed in caspase-8 knockdown HeLa cells compared to mock-treated or siNC-treated cells (Fig. 3B). These data suggested that caspase-8, rather than caspase-9, plays a dominant role in the dsRNA-triggered apoptosis.

Next, we tested whether AMBRA1 affects the activation of caspase-8 in poly(I:C)-treated A549 and HeLa cells. Upon poly(I:C) stimulation, the cleavage of caspase-8, caspase-3, and PARP in AMBRA1$^{KO}$ A549 cells was both dramatically decreased compared with that of control cells (Fig. 3C). Similar results were observed in AMBRA1$^{KO}$ HeLa cells (Fig. 3D), implying that AMBRA1 plays a role in caspase-8 activation.

In the dsRNA-triggered apoptosis pathway, the activation of caspase-8 was mediated by mitochondrial adaptor MAVS (El Maadidi et al., 2014; Li et al., 2009), which received the signal from RLR sensors (Kawai et al., 2005). As AMBRA1 is involved in the activation of caspase-8, and it partially locates in mitochondria (Strappazzon et al., 2011), we proposed that AMBRA1 probably functions through interacting with RLR sensors or their adaptor. To testify this hypothesis, we constructed plasmids expressing these sensors or adaptor, including RIG-I, MDA5, and MAVS. 293T cells were co-transfected with plasmid expressing AMBRA1-HA with plasmids expressing RIG-I-FLAG, MDA5-FLAG, MAVS-FLAG, or GFP-FLAG. At 24 h post-transfection, whole cell lysates were collected for co-immunoprecipitation (co-IP) assay. The data showed that AMBRA1-HA co-precipitated with MAVS-FLAG, but not RIG-I-FLAG and MDA5-FLAG (Fig. 3E). Interestingly, although two forms of MAVS, namely full-length (~72 kDa) and mini-MAVS (~50 kDa) (Brubaker et al., 2014) were present in the cell extracts (left panel, Fig. 3E), only the full-length MAVS (~72 kDa) was precipitated with AMBRA1-HA (right panel, Fig. 3E).

To confirm that endogenous AMBRA1 interacts with MAVS, we further performed co-IP assay using AMBRA1 antibody or MAVS antibody. As expected, the AMBRA1 antibody immunoprecipitated with AMBRA1 and MAVS; and reciprocally, the MAVS antibody immunoprecipitated with MAVS and AMBRA1 in A549 cells (Fig. 3F). Next, we examined the

localization of AMBRA1 and MAVS by immunofluorescence microscopy. 293T and HeLa cells were co-transfected with plasmids expressing AMBRA1-HA and MAVS-FLAG, and collected at 24 h for IFM assay using FLAG- and HA- antibodies. As shown in Fig. 3G, AMBRA1 (red) and MAVS (green) substantially colocalized in the cytoplasm. The intensity plot profile indicated a colocalization between AMBRA1 and MAVS (Fig. 3H) in both cells. These data demonstrated that AMBRA1 interacts with MAVS.

**TM domain of MAVS is indispensable for MAVS to interact with AMBRA1**

MAVS protein is composed of three domains, including CARD-like domain (CARD), proline-rich domain (Pro), and transmembrane domain (TM) (Ren et al., 2020). To map which domain of MAVS mediates the MAVS/AMBRA1 interaction, we generated a serial of constructs expressing MAVS truncates: 1-173-FLAG expressing 1-173 aa containing the CARD and Pro domains, Pro-FLAG expressing 78-173 aa containing Pro domain, and TM-FLAG expressing 174-540 aa containing TM domain (Fig. 4A). 293T cells were co-transfected with plasmids expressing AMBRA1-HA and MAVS truncates, and harvested for co-IP assay. Surprisingly, all truncates of MAVS did not interact with AMBRA1 (Fig. 4B). As a positive control, the full length MAVS was detected in the co-precipitated complex.

To further determine which domain of MAVS mediates the MAVS/AMBRA1 interaction, we utilized another panel of vectors expressing MAVS mutants fused to FLAG (Zhang et al., 2014). These vectors expressed full-length MAVS (MAVS-FLAG), MAVS lacking the CARD domain (ΔCARD-FLAG), MAVS lacking the Pro domain (ΔPro-FLAG), and MAVS lacking the TM domain (ΔTM-FLAG) respectively (Fig. 4C). 293T cells were co-transfected with plasmids expressing

AMBRA1-HA and MAVS truncates, and harvested for co-IP assay. Full-length MAVS-FLAG, ΔCARD-FLAG and ΔPro-FLAG, but not ΔTM-FLAG were co-precipitated with AMBRA1-HA (Fig. 4D), indicating the TM domain is critical for protein interaction.

**MAVS is crucial for AMBRA1 to promote the dsRNA-triggered apoptosis**

As AMBRA1 interacts with MAVS, and MAVS is the key mediator in the apoptosis induced by dsRNA (Yu et al., 2010), we hypothesized that the pro-apoptotic effect of AMBRA1 might rely on MAVS. To test this hypothesis, we generated MAVS$^{KO}$ A549 cells using CRISPR/Cas9 technique. Depletion of MAVS was confirmed by western blot (lane 5-8, Fig. 5A). The apoptosis extents were measured by western blot and flow cytometry. As expected, in response to poly(I:C), the cleavage of caspase-3 and PARP in MAVS$^{KO}$ was significantly lower than the control cells at indicated time points (Fig. 5A). The flow cytometry analysis revealed that the apoptosis percentage of MAVS$^{KO}$ cells (around 17%) was significantly reduced compared to the control cells (around 54%) (Fig. 5B), confirming a pro-apoptotic role of MAVS in dsRNA-treated A549 cells.

Next, we investigated whether MAVS depletion affects the regulatory effect of AMBRA1 on apoptosis. Cells were transduced with lentivirus expressing AMBRA1-HA into control, AMBRA1$^{KO}$, and MAVS$^{KO}$ cells, followed by blasticidin selection. The ectopic expression of AMBRA1-HA in selected cells was clearly detected by western blot using anti-AMBRA1 or anti-HA antibodies (Fig. 5C). Then, we compared the apoptosis extent induced by poly(I:C) in these cells by western blot. As shown in Fig. 5D, the cleavage of PARP, caspase-3, and caspase-8 was readily detected in the vector-transduced control cells upon poly(I:C) stimulation (lane 2), and was enhanced in the AMBRA1-HA expressing cells (lane 4). In the poly(I:C)-treated AMBRA1$^{KO}$ cells, the cleavage of

PARP, caspase-3, and caspase-8 in the AMBRA1-HA expressing cells (lane 8) was also increased compared to the vector-transduced cells (lane 6). The depletion of MAVS led to a significant reduction of PARP, caspase-3, and caspase-8 cleavage, regardless of whether AMBRA1-HA was absent (lane 10) or present (lane 12). The pro-apoptotic effect of AMBRA1 was abolished in the absence of MAVS, suggesting that the regulatory effect of AMBRA1 on the dsRNA-triggered apoptosis is mediated through MAVS.

**AMBRA1 maintains the stability of MAVS**

The observation that the pro-apoptotic effect of AMBRA1 relies on MAVS prompted us to examine whether their interaction is affected by dsRNA stimulation. A549 cells were transfected with mock or poly(I:C), and harvested for co-IP assay. Fig. 6A showed that in the whole cell extract, poly(I:C) led to reduction of MAVS levels, as a result of proteasomal degradation (Zhou et al., 2012). Still, more AMBRA1 was associated with MAVS upon poly(I:C)-stimulation (Fig. 6A). Based on this observation, we proposed that AMBRA1/MAVS interaction might have an influence on the MAVS stability. To test this hypothesis, we compared the protein levels of MAVS in the control and AMBRA1$^{KO}$ cells. Cells were transfected with mock or poly(I:C), and harvested at indicated time points for western blot. In the control cells, the MAVS levels were gradually decreased, consistent with previous report (Zhou et al., 2012). In the absence of AMBRA1, the MAVS levels were downregulated at higher extents (Fig. 6B and 6C), suggesting that AMBRA1 plays a role in maintaining the stability of MAVS. Of note, the mRNA levels of *MAVS* were comparable in the control and AMBRA1$^{KO}$ cells (data not shown).

To further confirm the role of AMBRA1 in stabilizing MAVS, we tested whether the MAVS expression was correlated with AMBRA1. 293T cells were co-transfected with fixed amount of plasmid expressing MAVS-FLAG, together with different doses of plasmid expressing AMBRA1-HA. At 24 h post-transfection, cells were collected for western blot or IFM assay. The AMBRA1-HA levels were increased when transfected with higher doses of plasmid. Interestingly, the MAVS-FLAG levels were also correlated with the dosages of plasmid expressing AMBRA1-HA (Fig. 6D). Consistently, the cell images showed that the percentages of MAVS-positive cells (green) were correlated with the percentages of AMBRA1-positive cells (red) (Fig. 6E). These data suggested that AMBRA1 might function in preventing the MAVS degradation through interacting it.

Since the degradation of MAVS upon poly(I:C) treatment is mediated by proteasome (Castanier et al., 2012; Zhou et al., 2012), we sought to explore whether AMBRA1 is involved in proteasomal degradation of MAVS. Cells were pretreated with MG132 for 1 h, an inhibitor of proteasome pathway, followed by poly(I:C) stimulation for 9 h. The degradation of MAVS in the control cells was abolished in the presence of MG132 (lane 2 and lane 6, Fig. 6F; black columns, Fig. 6G), indicating that the poly(I:C)-induced degradation of MAVS occurs through proteasome pathway in A549 cells. Consistent with Fig. 6B, the MAVS levels in AMBRA1$^{KO}$ cells were lower than the control cells after poly(I:C) stimulation (lane 2 and lane 4, Fig. 6F). Intriguingly, the MAVS levels in AMBRA1$^{KO}$ cells were restored to the level similar to that of the control cells in the presence of MG132 (lane 6 and lane 8, Fig. 6F). The levels of MAVS in the control and AMBRA1$^{KO}$ cells were comparable (MG132-treated group, Fig. 6G). These data indicated that AMBRA1 probably stabilizes MAVS by blocking the poly(I:C)-mediated proteasomal degradation of MAVS.

**AMBRA1 promotes the apoptosis induced by SFV infection**

To explore whether AMBRA1 plays a role in virus-induced apoptosis, we utilized SFV as an infection model. SFV is an enveloped, single-stranded positive RNA virus, and it leads to apoptosis through producing dsRNA during replication (El Maadidi et al., 2014). The control, AMBRA1$^{KO}$, AMBRA1$^{RES}$, and MAVS$^{KO}$ A549 cells were infected with SFV at a multiplicity of infection (MOI) of 1. At 6 h and 12 h post infection (p.i.), the cells were harvested for SFV RNA levels analysis by qRT-PCR. The RNA levels of SFV in all tested cells were comparable at indicated time points (Fig. 7A), indicating that AMBRA1 or MAVS depletion does not alter the viral RNA replication prior to 12 h p.i. At 48 h p.i., typical apoptosis characteristics including severe membrane blebbing and cell shrinkage were visualized in control A549 cells (Fig. S3A). As expected, the morphological changes of two AMBRA1$^{KO}$ clones or MAVS$^{KO}$ cells were less severe than the control and AMBRA1$^{RES}$ cells upon SFV infection (Fig. S3A), indicating that AMBRA1 and MAVS are involved in the SFV-induced apoptosis.

Next, we evaluated role of AMBRA1 or MAVS in the SFV-induced apoptosis by western blot and flow cytometry. In the SFV-infected AMBRA1$^{KO}$ and MAVS$^{KO}$ cells, the ratio of c-caspase-3/caspase-3, and the cleavage of PARP and caspase-8 were decreased compared to the control or AMBRA1$^{RES}$ cells (Fig. 7B). The flow cytometry analysis showed that the percentages of apoptotic cells were significantly reduced in two AMBRA1$^{KO}$ cell clones compared with the control and AMBRA1$^{RES}$ cells at 24 h p.i. and 48 h p.i. (Fig. 7C and 7D). As expected, the apoptosis extents in MAVS$^{KO}$ were also dramatically reduced (Fig. 7C and 7D). These data suggested that AMBRA1 and MAVS positively regulate apoptosis induced by SFV. Then, we tested whether AMBRA1 or MAVS depletion has an impact on the late stage replication level of SFV. The control, AMBRA1$^{KO}$,

AMBRA1$^{RES}$, and MAVS$^{KO}$ cells were infected with SFV and harvested at 24 h p.i. for plaque assay. The viral yields in the AMBRA1$^{KO}$ and MAVS$^{KO}$ cells were enhanced by about 10-fold and 4.5-fold respectively, compared to the control cells (Fig. S3B). These data implied that AMBRA1 and MAVS promoted the SFV-induced apoptosis, which might help to block the viral production.

## DISCUSSION

AMBRA1 has been indicated to modulate the autophagic pathway and apoptosis induced by various stimuli (Di Bartolomeo et al., 2010; Fimia et al., 2007; Gu et al., 2014; Li et al., 2016; Liu et al., 2019; Pagliarini et al., 2012; Strappazzon et al., 2016; Sun et al., 2018; Sun et al., 2019). Nonetheless, whether AMBRA1 plays a role in the cellular responses to virus remains uninvestigated. This study provides first view of AMBRA1 regulation in the apoptosis induced by dsRNA or virus. Several important findings emerged from our study.

First, we found that AMBRA1 positively regulates the dsRNA-induced apoptosis. The knockout of AMBRA1 resulted in less cell death induced by poly(I:C) or SFV, a virus which triggers apoptosis through producing dsRNA (El Maadidi et al., 2014), and complementation of AMBRA1 restored the extent of cell death. Furthermore, we determined that AMBRA1 is a positive regulator of apoptosis induced by dsRNA or SFV, supported by the data obtained from the apoptosis inhibitor (zVAD) assay, as well as apoptosis measurements (caspase-3 and PARP cleavage, karyopyknosis, and percentage of apoptotic cells). Although AMBRA1 has been reported to regulate apoptosis in different contexts, our work first established an association of AMBRA1 and apoptosis induced by virus or dsRNA which mimics viral byproduct. Intriguingly, the AMBRA1 depletion does not affect the cell death induced by $H_2O_2$ or UV (data not shown), suggesting that AMBRA1-mediated

apoptosis is stimuli-dependent. AMBRA1 is also a key regulator of autophagy. Interestingly, we found that the extent of autophagy in the AMBRA1$^{KO}$ cells was more significant compared to the control cells by detecting protein levels of two indicators of autophagy, p62 and LC3 II converted from LC3 I (Fig. S2E), suggesting that AMBRA1 downregulates the dsRNA-induced autophagy, in accordance with the fact that AMBRA1 promotes dsRNA-induced apoptosis.

Mechanistically, our study associated AMBRA1 with MAVS, a key regulator of apoptosis induced by virus (Kawai et al., 2005). First, our study demonstrated an interaction between AMBRA1/MAVS and further mapped the region of MAVS required for their interaction. The co-IP and IFM data demonstrated that AMBRA1 interacts and co-localized with mitochondrial MAVS. Importantly, we found that the TM domain of MAVS is indispensable for their interaction, suggesting that the mitochondria-localization of MAVS is crucial. Moreover, most individual regions of MAVS except for TM domain, including N-terminal domain (1-173 aa), Pro domain (78-173 aa), and C-terminal domain (174-540 aa) were not sufficient to mediate their interaction. In combination with that ΔCARD lacking 1-92 aa and ΔPro lacking 104-172 aa binds to AMBRA1, we proposed that 93-103 aa fragment of MAVS, might be the key region mediating their interaction. Particularly, the interaction between MAVS and AMBRA1 was strengthened by poly(I:C) stimulation despite less MAVS was present in the stimulated cells, illustrating a biological significance of their interaction.

Then, we found that the pro-apoptotic effect of AMBRA1 relies on the presence of MAVS. MAVS plays an essential role in the apoptosis stimulated by dsRNA or SFV in A549 cells, consistent with previous reports (El Maadidi et al., 2014; Kumar et al., 2015; McAllister and Samuel, 2009). Interestingly, the pro-apoptotic effect of AMBRA1 is largely abolished in poly(I:C)-treated MAVS$^{KO}$ cells, indicating that the pro-apoptotic effect of AMBRA1 depends on MAVS. As the mitochondria

localization of MAVS is critical for apoptosis induction (Okazaki et al., 2013) and for its interaction with AMBRA1, the function of AMBRA1 might be executed through mitochondrial MAVS.

We demonstrated that AMBRA1 prevents MAVS from proteasomal degradation. In the AMBRA1$^{KO}$ cells, the MAVS protein levels but not its mRNA levels were decreased more rapidly in the context of dsRNA stimulation, and MAVS protein was expressed at higher levels along with higher doses of AMBRA1, strongly suggesting that AMBRA1 is important for maintaining the MAVS stability. When treated with proteasomal inhibitor MG132, the MAVS levels in poly(I:C)-treated control cells were similarly increased as in poly(I:C)-treated AMBRA1$^{KO}$ cells, indicating that AMBRA1 helps to prevent the proteasome-mediated degradation of MAVS, which is similar to its role in stabilizing ULK1 (Nazio et al., 2013). Therefore, we illustrated a new mechanism that AMBRA1 upregulates the apoptosis through stabilizing IPS-1 (MAVS), which differs from the report showing AMBRA1 promotes apoptosis through binding and inactivating anti-apoptosis BCL2 (Strappazzon et al., 2016)

Furthermore, our data revealed that AMBRA1 is involved in the activation of caspase-8 induced by dsRNA. The pan-caspase inhibitor, zVAD, abolished the poly(I:C)-induced apoptosis, consistent with previous study showing caspase is essential in this pathway (Salaun et al., 2006). Further RNAi study demonstrated that caspase-8 and caspase-9, two main initiators in the apoptosis pathway, played differential roles in the dsRNA-induced apoptosis pathway. Caspase-8 knockdown in A549 and HeLa cells led to less apoptosis, in keeping with the observation that inhibition of caspase-8 efficiently blocks the cleavage of PARP in dsRNA-treated HeLa cells (Iordanov et al., 2005), while knockdown of caspase-9 did not alter the cleavage of PARP in poly(I:C)-treated A549 and HeLa cells. Intriguingly, some studies reported that caspase-9 is required for apoptosis triggered in

poly(I:C)-treated SK-N-AS cells, AfMNPV-treated Sl-1 cells, and silica- and poly(I:C)-induced NHBE cells (Chuang et al., 2012; Liu et al., 2012; Unno et al., 2014). These discrepancies suggested that role of caspase-9 might be stimuli and cell specific, and in some cell types, alternative pathway might exist, so caspase-9 knockdown alone does not show an alteration of apoptosis. In addition, depletion of either AMBRA1 or MAVS significantly affected the cleavage of caspase-8, demonstrating that they function at upstream of caspase-8 activation. As poly(I:C) triggers production of TNFα in Dendritic cells (Kobayashi et al., 2013), which might elicit caspase-8-dependent apoptosis, we also tested whether the pro-apoptotic role of AMBRA1 is mediated through regulating TNFα. We found the TNFα level in A549 cells was only enhanced by 2-fold upon poly(I:C) stimulation, and treatment of TNFα did not elicit apoptosis in A549 cells (data not shown). Therefore, an involvement of a paracrine effect of TNFα in AMBRA1-regulated apoptosis was ruled out.

Given the role of AMBRA1 in stabilizing MAVS and activating caspase-8, we proposed that AMBRA1 mediates apoptosis through regulating the recruitment and activation of caspase-8 by MAVS. MAVS has been shown to regulate the apoptosis through various mechanisms, one of which is by recruiting and activating caspase-8 (El Maadidi et al., 2014; Li et al., 2009). As AMBRA1 interacts with MAVS, and AMBRA1 promotes the activation of caspase-8, we deduced that AMBRA1 has an impact on the interaction between MAVS and caspase-8, which benefits the cleavage and activation of caspase-8 (El Maadidi et al., 2014; Li et al., 2009).

In conclusion, our work identified AMBRA1 as a new regulator involved in apoptosis induced by poly(I:C) and SFV. Furthermore, we illustrated that AMBRA1 interacts with MAVS and prevents its proteasomal degradation, thereby facilitating the activation of caspase-8 (Fig. 8). Therefore, our work established a relationship between AMBRA1 and MAVS, a central molecule in the cellular response to viral infection, and revealed a new mechanism of AMBRA1 in the apoptosis.

## MATERIALS AND METHODS

### Cells and reagents

Human lung carcinoma epithelial cells (A549, ATCC CCL-185), human cervical cancer cells (HeLa，ATCC CCL-2) and human embryonic kidney cells (293T, ATCC CRL-3216) were maintained in Dulbecco Modified Eagle Medium (DMEM, Gibco) supplemented with 10% fetal bovine serum (FBS) (Gibco) at 37 °C in an incubator with 5% $CO_2$. African green monkey kidney cells (Vero, ATCC CCL-81) were maintained in DMEM supplemented with 5% FBS at 37 °C in an incubator with 5% $CO_2$. *Aedes albopictus* cells (C6/36, ATCC CRL-1660) were maintained in RPMI 1640 medium (Gibco) supplemented with 10% FBS (Gibco) and NEAA (Gibco) at 28 °C in an incubator with 5% $CO_2$. The media were added with 100 units/ml of streptomycin and penicillin (Invitrogen). Poly(I:C) and puromycin was purchased from Sigma; z-VAD(OMe)-FMK, Necrostatin-1, Necrosulfonamide, and MG132 were purchased from MCE; Lipofectamine 2000 Reagent was purchased from Invitrogen. Blasticidin was purchased from Invivogen.

**Virus, virus propagation, titration, and virus infection**

Semliki forest virus was kindly provided by Dr. Zhou Xi (Qian et al., 2020). It was propagated by infecting the C6/36 cells with a multiplicity of infection (MOI) of 20. After culturing at 28 °C for 24 h, the supernatant was harvested and centrifuged to remove cell debris. The supernatant was stored at -80 °C. Virus titers of SFV were determined by a standard plaque assay. In the plaque assay, Vero cells in 12-well plates were infected with a 10-fold serial dilution of viruses. The cells were cultured at 37 °C for 2 h to allow the adsorption of all viruses. The supernatant was then replaced with the mixture of 2 × DMEM containing 20% FBS and 2% penicillin-streptomycin and isopycnic 2% low melting point agarose (Sigma) (1:1). After incubation at 37 °C for 24 h, the cells were fixed with 10% formaldehyde and stained with 0.5% crystal violet.

Cells were infected with SFV at an MOI of 1 in DMEM without FBS. Cells were harvested at indicated time points for qRT-PCR, western blot or flow cytometry detection.

**Antibodies**

Primary antibodies included anti-p62 (Santa Cruz Inc.), anti-β-actin (Sigma), anti-cleaved PARP (CST), anti-caspase-3 (CST), anti-p62 (CST), anti-LC3 I/II (MBL), anti-α-tubulin (BBI Life Science), anti-AMBRA1 (Santa Cruz Inc.), anti-MAVS (Santa Cruz Inc.), anti-HA (MBL), and anti-FLAG (MBL), anti-caspase-8 (proteintech), anti-caspase-9 (proteintech) and anti-c-caspase-8 (CST). Secondary antibodies included IRDye 800 CW-conjugated anti-rabbit IgG, IRDye 680 CW-conjugated anti-mouse IgG (LI-COR), horseradish peroxidase (HRP)-conjugated anti-mouse IgG (CST), and anti-rabbit IgG (Bio-Rad). Secondary antibodies for immunofluorescence assay

included Goat anti-Rabbit Secondary Antibody (Alexa Fluor 488) and Goat anti-Mouse Secondary Antibody (Alexa Fluor 647) from Invitrogen.

**Generation of AMBRA1 and MAVS knockout cell clones**

AMBRA1 and MAVS knockout cell clones were generated using CRISPR/Cas9 technique (Ran et al., 2013). sgRNAs targeting *AMBRA1* and *MAVS* were cloned into lentiCRISPR v2 (Addgene #52961). Sequences of sgRNAs are listed in Table S1 (Supplemental data). Lentiviruses were packaged in 293T cells. LentiCRISPR v2 containing single sgRNA, along with pSPAX2 (Addgene #12260) and pVSVG (Addgene #12259), were introduced into 293T cells using FuGENE® HD Reagent (Promega). After 2 days, culture supernatants were passed through a 0.45 μm filter, and used for gene transduction. A549 and HeLa cells were transduced with lentiviruses expressing single sgRNA and selected by puromycin (1 μg/ml), and single clones were isolated. AMBRA1 knockout cell clones were confirmed by Sanger sequencing, and mRNA levels of *AMBRA1* were measured by qRT-PCR. Genomic DNA was extracted using a genomic DNA extraction kit (Bioteke). Regions surrounding sgRNA target sequence were amplified by PCR and then PCR products were cloned into pMD-18T (TaKaRa) for Sanger sequencing. Sequences of primers were listed in Table S2 (Supplemental data).

**Generation of AMBRA1$^{RES}$ cells and stably expression of exogenous AMBRA1 in AMBRA1$^{KO}$ and MAVS$^{KO}$ cells**

The *AMBRA1* gene fragment was amplified by PCR and cloned into the lentivirus vector CSII-EF-MCS-IRES2-Venus (Riken RDB04384) or pLV-EF1α-IRES-Blast (Addgene #85133). Primer sequences used were listed in Table S2 (Supplemental data). Lentiviruses were packaged in

293T cells. pLV-EF1α-IRES-Blast-AMBRA1 or CSII-EF-MCS-IRES2-Venus-AMBRA1, along with pSPAX2 (Addgene #12260) and pVSVG (Addgene #12259), were introduced into 293T cells using FuGENE® HD Reagent. After 2 days, culture supernatants were collected and passed through a 0.45 μm filter, and used for gene transduction. AMBRA1$^{KO}$ cells were transduced with lentivirus carrying *AMBRA1* gene (CSII-EF-MCS-IRES2-Venus), and Venus positive cells were sorted as AMBRA1$^{RES}$ cells by flow cytometry (BD). AMBRA1$^{KO}$ or MAVS$^{KO}$ cells were transduced with lentivirus carrying *AMBRA1* gene (pLV-EF1α-IRES-Blast), and then selected by Blasticidin (15 μg/ml) for 1 week.

**Quantitative real time-PCR (qRT-PCR)**

Total RNAs were reverse transcribed using HI Script Q RT SuperMix (Vazyme). The cDNA was used as the template for qRT-PCR. The qRT-PCR was performed using SYBR Select Master Mix for CFX (Applied Bio systems) in Bio-Rad CFX96 machine. The PCR data were analyzed using SDS software (Applied Biosystems). The mRNA level of *β-actin* was measured as an internal control. The primers for qRT-PCR were listed in Table S3 (Supplemental data).

**Plasmid construction and transfection**

To amplify full-length of *AMBRA1*, *MDA5*, and *RIG-I*, cDNA prepared from A549 cells was used as template. The PCR primers were listed in Table S2 (Supplemental data). 1-173-FLAG expressing aa 1-173 containing the CARD and Pro domains, was amplified using the full-length MAVS. Pro-FLAG and TM-FLAG were gifts from Dr. Zhu Xun in School of Medicine, Sun Yat-Sen University (Hu et al., 2019). The amplified fragments were purified and cloned into pSG5 vector. All

plasmids were transfected into cells using Lipofectamine 2000 Reagent following the manufacturer's instructions.

**Treatment of poly(I:C) and cell imaging**

Cells were seeded in 12-well plates. Poly(I:C) (1 μg/ml) was transfected into cells using Lipofectamine 2000 Reagent in all experiments according to the protocols provided by the manufacturer. At 24 h post-transfection, photographs were taken using Leica DMi8.

**MTT assay**

MTT (3-(4,5)-dimethylthiahiazo (-z-y1)-3,5-di-phenytetrazoliumromide, Genview) was dissolved in PBS at a concentration of 5 mg/ml before use. The cells were incubated in the presence of MTT for 4 h. After centrifugation at 1500 rpm for 5 min, the supernatant was discarded and DMSO was added to the plate, followed by 10-minute gentle shake. OD value was measured at 490 nm using a BioTek Instrument (BioTek).

**CCK8 assay**

Cell Counting Kit-8 (CCK8) was purchased from MCE. 80 μL reagent was added to cell culture (12-well plate) and incubated in the incubator (37 °C with 5% $CO_2$). 1 h later, the OD value was measured at 450 nm using a BioTek Instrument (BioTek).

**Western blot**

Cells were lysed in RIPA lysis buffer (pH 7.4) (50 mM Tris-HCl, 0.5% [v/v] NP-40, 1% Triton-100, 150 mM NaCl, 1 mM EDTA, 1 mM PMSF, 1% protease inhibitor cocktails (Sigma), 1 mM $Na_3VO_4$, and 1 mM NaF). Proteins were separated on SDS-PAGE and transferred onto nitrocellulose membranes. The membranes were blocked in PBST with 5% bovine serum albumin (BSA) (New England Biolabs) and incubated with indicated primary antibodies at 4 °C overnight. IRDye 800 CW-conjugated anti-rabbit IgG (LI-COR), IRDye 680 CW-conjugated anti-mouse IgG (LI-COR) or horseradish peroxidase-conjugated secondary antibodies (Bio-Rad) served as secondary antibodies. Detection was performed according to the manufacturer's protocols.

**Inhibitor assay**

z-VAD(OMe)-FMK (zVAD) and Necrostatin-1 (Necro-1) were dissolved in DMSO at a stock concentration of 100 mM. Necrosulfonamide (NSA) and MG132 were dissolved in DMSO at a stock concentration of 5 mM and 40 mM, respectively. Cells were pretreated with 50 μM zVAD, 100 μM Necro-1, their combination or indicated concentration of NSA for 1 h. Cells were transfected with poly(I:C) along with DMSO or these inhibitors respectively.

Cells were pretreated with DMSO or 10 μM of MG132 for 1 h, followed by poly(I:C) transfection.

**RNA interference**

The sequences of siRNAs targeting human *caspase-8* mRNA and *caspase-9* mRNA were 5'-GUCAUGCUCUAUCAGAUUU-3' and 5'-GUCGAAGCCAACCCUAGAA-3', respectively. A control siRNA with scrambled sequence was used as negative control (siNC). Transfection was

carried out with 16 nmol of siRNAs by using Lipofectamine 2000 Reagent according to the manufacturer's instructions. At 48 h post-transfection, cells were harvested for further analysis.

**Flow cytometry**

Apoptotic cells were assessed by Annexin V-PE/7-AAD detection. Cells were seeded into 12-well plates, and then transfected with poly(I:C) or infected with SFV at an MOI of 1. At 12 h post-transfection or indicated time points of SFV infection, cells were collected by centrifugation, washed with cold PBS, and subsequently resuspended in 100 μl of 1 × Binding Buffer prior to incubation with 2.5 μl Annexin V-PE and 2.5 μl 7-AAD (BD). The specimens were incubated on ice for 15 min, and then 300 μl of 1 × Binding Buffer was added to dilute the cell suspension. Subsequently the portions of apoptotic cells were detected by a flow cytometer (Beckman CytoFLEX, USA).

**Confocal assay**

Cells were washed with PBS and fixed with 4% (v/v) paraformaldehyde, permeabilized with 0.02% Triton X-100, and then blocked in PBS with 5% bovine serum albumin (BSA) for 1 h. Cells were incubated with primary antibodies at 4 °C overnight. Cells were incubated for 1 h with Alexa Fluor 647-conjugated goat anti-mouse-IgG (Invitrogen) and Alexa Fluor 488-conjugated anti-rabbit-IgG (ThermoFisher) at room temperature. Cells were stained with 4',6-diamidino-2-phenylindole (DAPI) (Invitrogen, CA). Fluorescent images were captured on a Nikon Eclipse Ni-E microscope.

**Co-immunoprecipitation (co-IP)**

293T cells were co-transfected with AMBRA1-HA and the indicated plasmids tagging with FLAG. At 24 h post-transfection, whole-cell lysates were harvested with RIPA lysis buffer. Lysates were incubated on ice for 30 min and then spun for 15 min at 4 °C. 20 μl of anti-HA beads (Sigma) was added to the cell lysate and incubated overnight. The beads were washed with wash buffer (50 mM Tris-HCl, 150 mM NaCl, 1 mM EDTA, 0.5% NP40), and then the precipitated proteins were eluted by boiling in the loading buffer, and detected by western blot.

To detect the physical interaction between endogenous AMBRA1 and MAVS, A549 cells lysates were prepared with RIPA lysis buffer. The co-IP assay was performed using protein A/G agarose (Calbiochem) along with antibodies for AMBRA1 or MAVS, IgG serving as a negative control.

**Statistical analysis**

All the data were shown as means ± standard deviations (SD) from at least three independent experiments. Data were analyzed with GraphPad Prism 7.0 software. The statistical analysis was performed with ANOVA with Dunnett's multiple comparison test or with an unpaired, two-tailed Student's *t* test, and the differences were considered statistically significant when $p$ was $<0.05$.

**Acknowledgements**

We thank Dr. Zhou Xi (Wuhan University, Wuhan, China) for generously providing Semliki Forest virus. We thank Dr. Zhang Rong (Fudan University, Shanghai, China) for kindly providing pLV-EF1α-IRES-Blast vector, and we thank Dr. Zhu Xun (Sun Yat-sen University, Guangzhou, China) for kindly providing two plasmids, Pro-FLAG and TM-FLAG.

## Competing interests

The authors declare no competing interests.

## Author contributions

P.Z., C.L., Y.L., C.H. and H.G. conceived and designed this project; Y.L. and C.H. performed most of the experiments and analyzed the results; X.L. and Z.H. participated in some experiments; Y.L. and H.G. conducted background investigation and data analysis; Q.L., S.Z. and Y.H. provided useful advice on methodology and data analysis; P.Z. and Y.L. wrote the manuscript; P.Z. and C.L. revised the manuscript. All the authors read and approved the manuscript.


## Funding

This work was supported by National Natural Science Foundation of China (31970887), Guangdong Science and Technology Program (2018A050506029), and Natural Science Foundation of Guangdong Province (2020A1515010870, 2021A1515011491).


# REFERENCES


**Amarante-Mendes, G. P., Adjemian, S., Branco, L. M., Zanetti, L. C., Weinlich, R. and Bortoluci, K. R.** (2018). Pattern Recognition Receptors and the Host Cell Death Molecular Machinery. *Front Immunol* **9**, 2379.

**Barber, G. N.** (2005). The dsRNA-dependent protein kinase, PKR and cell death. *Cell Death Differ* **12**, 563-70.

**Brubaker, S. W., Gauthier, A. E., Mills, E. W., Ingolia, N. T. and Kagan, J. C.** (2014). A bicistronic MAVS transcript highlights a class of truncated variants in antiviral immunity. *Cell* **156**, 800-11.

**Budihardjo, I., Oliver, H., Lutter, M., Luo, X. and Wang, X.** (1999). Biochemical pathways of caspase activation during apoptosis. *Annu Rev Cell Dev Biol* **15**, 269-90.

**Castanier, C., Zemirli, N., Portier, A., Garcin, D., Bidere, N., Vazquez, A. and Arnoult, D.** (2012). MAVS ubiquitination by the E3 ligase TRIM25 and degradation by the proteasome is involved in type I interferon production after activation of the antiviral RIG-I-like receptors. *Bmc Biology* **10**.

**Castelli, J. C., Hassel, B. A., Wood, K. A., Li, X. L., Amemiya, K., Dalakas, M. C., Torrence, P. F. and Youle, R. J.** (1997). A study of the interferon antiviral mechanism: apoptosis activation by the 2-5A system. *J Exp Med* **186**, 967-72.

**Chattopadhyay, S. and Sen, G. C.** (2017). RIG-I-like receptor-induced IRF3 mediated pathway of apoptosis (RIPA): a new antiviral pathway. *Protein Cell* **8**, 165-168.

**Chawla-Sarkar, M., Lindner, D. J., Liu, Y. F., Williams, B., Sen, G. C., Silverman, R. H. and Borden, E. C.** (2003). Apoptosis and interferons: Role of interferon-stimulated genes as mediators of apoptosis. *Apoptosis* **8**, 237-249.

**Chiramel, A. I., Brady, N. R. and Bartenschlager, R.** (2013). Divergent roles of autophagy in virus infection. *Cells* **2**, 83-104.

**Chuang, J. H., Lin, T. K., Tai, M. H., Liou, C. W., Huang, S. T., Wu, C. L., Lin, H. Y. and Wang, P. W.** (2012). Preferential involvement of mitochondria in Toll-like receptor 3 agonist-induced neuroblastoma cell apoptosis, but not in inhibition of cell growth. *Apoptosis* **17**, 335-348.

**Creagh, E. M., Conroy, H. and Martin, S. J.** (2003). Caspase-activation pathways in apoptosis and immunity. *Immunol Rev* **193**, 10-21.

**Di Bartolomeo, S., Corazzari, M., Nazio, F., Oliverio, S., Lisi, G., Antonioli, M., Pagliarini, V., Matteoni, S., Fuoco, C., Giunta, L. et al.** (2010). The dynamic interaction of AMBRA1 with the dynein motor complex regulates mammalian autophagy. *J Cell Biol* **191**, 155-68.

**El Maadidi, S., Faletti, L., Berg, B., Wenzl, C., Wieland, K., Chen, Z. J., Maurer, U. and Borner, C.** (2014). A novel mitochondrial MAVS/Caspase-8 platform links RNA virus-induced innate antiviral signaling to Bax/Bak-independent apoptosis. *J Immunol* **192**, 1171-83.

**Fimia, G. M., Di Bartolomeo, S., Piacentini, M. and Cecconi, F.** (2011). Unleashing the Ambra1-Beclin 1 complex from dynein chains: Ulk1 sets Ambra1 free to induce autophagy. *Autophagy* **7**, 115-7.

**Fimia, G. M., Stoykova, A., Romagnoli, A., Giunta, L., Di Bartolomeo, S., Nardacci, R., Corazzari, M., Fuoco, C., Ucar, A., Schwartz, P. et al.** (2007). Ambra1 regulates autophagy and development of the nervous system. *Nature* **447**, 1121-5.

**Gao, H., Lin, Y., He, J., Zhou, S., Liang, M., Huang, C., Li, X., Liu, C. and Zhang, P.** (2019). Role of heparan sulfate in the Zika virus entry, replication, and cell death. *Virology* **529**, 91-100.

**Gu, W., Wan, D., Qian, Q., Yi, B., He, Z., Gu, Y., Wang, L. and He, S.** (2014). Ambra1 is an essential regulator of autophagy and apoptosis in SW620 cells: pro-survival role of Ambra1. *PLoS One* **9**, e90151.

**Hu, Y. W., Dong, X. H., He, Z. J., Wu, Y., Zhang, S. H., Lin, J. J., Yang, Y., Chen, J. H., An, S., Yin, Y. X. et al.** (2019). Zika virus antagonizes interferon response in patients and disrupts RIG-I-MAVS interaction through its CARD-TM domains. *Cell and Bioscience* **9**.

**Imre, G.** (2020). Cell death signalling in virus infection. *Cell Signal* **76**, 109772.

**Iordanov, M. S., Ryabinina, O. P., Schneider, P. and Magun, B. E.** (2005). Two mechanisms of caspase 9 processing in double-stranded RNA- and virus-triggered apoptosis. *Apoptosis* **10**, 153-66.

**Jordan, T. X. and Randall, G.** (2012). Manipulation or capitulation: virus interactions with autophagy. *Microbes Infect* **14**, 126-39.

**Kawai, T., Takahashi, K., Sato, S., Coban, C., Kumar, H., Kato, H., Ishii, K. J., Takeuchi, O. and Akira, S.** (2005). IPS-1, an adaptor triggering RIG-I- and Mda5-mediated type I interferon induction. *Nat Immunol* **6**, 981-8.

**Kobayashi, Y., Iwata, A., Suzuki, K., Suto, A., Kawashima, S., Saito, Y., Owada, T., Kobayashi, M., Watanabe, N. and Nakajima, H.** (2013). B and T lymphocyte attenuator inhibits LPS-induced endotoxic shock by suppressing Toll-like receptor 4 signaling in innate immune cells. *Proc Natl Acad Sci U S A* **110**, 5121-6.

**Kumar, S., Ingle, H., Mishra, S., Mahla, R. S., Kumar, A., Kawai, T., Akira, S., Takaoka, A., Raut, A. A. and Kumar, H.** (2015). IPS-1 differentially induces TRAIL, BCL2, BIRC3 and PRKCE in type I interferons-dependent and -independent anticancer activity. *Cell Death Dis* **6**, e1758.

**Li, H. M., Fujikura, D., Harada, T., Uehara, J., Kawai, T., Akira, S., Reed, J. C., Iwai, A. and Miyazaki, T.** (2009). IPS-1 is crucial for DAP3-mediated anoikis induction by caspase-8 activation. *Cell Death and Differentiation* **16**, 1615-1621.

**Li, X., Zhang, L., Yu, L., Wei, W., Lin, X., Hou, X. and Tian, Y.** (2016). shRNA-mediated AMBRA1 knockdown reduces the cisplatin-induced autophagy and sensitizes ovarian cancer cells to cisplatin. *J Toxicol Sci* **41**, 45-53.

**Liu, J., Chen, Z., Guo, J., Wang, L. and Liu, X.** (2019). Ambra1 induces autophagy and desensitizes human prostate cancer cells to cisplatin. *Biosci Rep* **39**.

**Liu, K., Shu, D., Song, N., Gai, Z., Yuan, Y., Li, J., Li, M., Guo, S., Peng, J. and Hong, H.** (2012). The role of cytochrome c on apoptosis induced by Anagrapha falcifera multiple nuclear polyhedrosis virus in insect Spodoptera litura cells. *PLoS One* **7**, e40877.

**McAllister, C. S. and Samuel, C. E.** (2009). The RNA-activated protein kinase enhances the induction of interferon-beta and apoptosis mediated by cytoplasmic RNA sensors. *J Biol Chem* **284**, 1644-51.

**McCormick, C. and Khaperskyy, D. A.** (2017). Translation inhibition and stress granules in the antiviral immune response. *Nat Rev Immunol* **17**, 647-660.

**Nagata, S. and Tanaka, M.** (2017). Programmed cell death and the immune system. *Nat Rev Immunol* **17**, 333-340.

**Nazio, F., Strappazzon, F., Antonioli, M., Bielli, P., Cianfanelli, V., Bordi, M., Gretzmeier, C., Dengjel, J., Piacentini, M., Fimia, G. M. et al.** (2013). mTOR inhibits autophagy by controlling ULK1 ubiquitylation, self-association and function through AMBRA1 and TRAF6. *Nature Cell Biology* **15**, 406-+.

**Okazaki, T., Higuchi, M. and Gotoh, Y.** (2013). Mitochondrial localization of the antiviral signaling adaptor IPS-1 is important for its induction of caspase activation. *Genes to Cells* **18**, 493-501.

**Pagliarini, V., Wirawan, E., Romagnoli, A., Ciccosanti, F., Lisi, G., Lippens, S., Cecconi, F., Fimia, G. M., Vandenabeele, P., Corazzari, M. et al.** (2012). Proteolysis of Ambra1 during apoptosis has a role in the inhibition of the autophagic pro-survival response. *Cell Death Differ* **19**, 1495-504.

**Pasparakis, M. and Vandenabeele, P.** (2015). Necroptosis and its role in inflammation. *Nature* **517**, 311-20.

**Qian, Q., Zhou, H., Shu, T., Mu, J., Fang, Y., Xu, J., Li, T., Kong, J., Qiu, Y. and Zhou, X.** (2020). The Capsid Protein of Semliki Forest Virus Antagonizes RNA Interference in Mammalian Cells. *J Virol* **94**.

**Ran, F. A., Hsu, P. D., Wright, J., Agarwala, V., Scott, D. A. and Zhang, F.** (2013). Genome engineering using the CRISPR-Cas9 system. *Nature Protocols* **8**, 2281-2308.

**Rathkey, J. K., Zhao, J., Liu, Z., Chen, Y., Yang, J., Kondolf, H. C., Benson, B. L., Chirieleison, S. M., Huang, A. Y., Dubyak, G. R. et al.** (2018). Chemical disruption of the pyroptotic pore-forming protein gasdermin D inhibits inflammatory cell death and sepsis. *Sci Immunol* **3**.

**Ren, Z., Ding, T., Zuo, Z., Xu, Z., Deng, J. and Wei, Z.** (2020). Regulation of MAVS Expression and Signaling Function in the Antiviral Innate Immune Response. *Front Immunol* **11**, 1030.

**Salaun, B., Coste, I., Rissoan, M. C., Lebecque, S. J. and Renno, T.** (2006). TLR3 can directly trigger apoptosis in human cancer cells. *Journal of Immunology* **176**, 4894-4901.

**Sanjo, H., Nakayama, J., Yoshizawa, T., Fehling, H. J., Akira, S. and Taki, S.** (2019). Cutting Edge: TAK1 Safeguards Macrophages against Proinflammatory Cell Death. *J Immunol* **203**, 783-788.

**Shi, J., Zhao, Y., Wang, K., Shi, X., Wang, Y., Huang, H., Zhuang, Y., Cai, T., Wang, F. and Shao, F.** (2015). Cleavage of GSDMD by inflammatory caspases determines pyroptotic cell death. *Nature* **526**, 660-5.

**Son, K. N., Liang, Z. G. and Lipton, H. L.** (2015). Double-Stranded RNA Is Detected by Immunofluorescence Analysis in RNA and DNA Virus Infections, Including Those by Negative-Stranded RNA Viruses. *Journal of Virology* **89**, 9383-9392.

**Strappazzon, F., Di Rita, A., Cianfanelli, V., D'Orazio, M., Nazio, F., Fimia, G. M. and Cecconi, F.** (2016). Prosurvival AMBRA1 turns into a proapoptotic BH3-like protein during mitochondrial apoptosis. *Autophagy* **12**, 963-975.

**Strappazzon, F., Vietri-Rudan, M., Campello, S., Nazio, F., Florenzano, F., Fimia, G. M., Piacentini, M., Levine, B. and Cecconi, F.** (2011). Mitochondrial BCL-2 inhibits AMBRA1-induced autophagy. *EMBO J* **30**, 1195-208.

**Sun, L., Wang, H., Wang, Z., He, S., Chen, S., Liao, D., Wang, L., Yan, J., Liu, W., Lei, X. et al.** (2012). Mixed lineage kinase domain-like protein mediates necrosis signaling downstream of RIP3 kinase. *Cell* **148**, 213-27.

**Sun, W. L., Wang, L., Luo, J., Zhu, H. W. and Cai, Z. W.** (2018). Ambra1 modulates the sensitivity of breast cancer cells to epirubicin by regulating autophagy via ATG12. *Cancer Sci* **109**, 3129-3138.

**Sun, W. L., Wang, L., Luo, J., Zhu, H. W. and Cai, Z. W.** (2019). Ambra1 inhibits paclitaxel-induced apoptosis in breast cancer cells by modulating the Bim/mitochondrial pathway. *Neoplasma* **66**, 377-385.

**Takaki, H., Shime, H., Matsumoto, M. and Seya, T.** (2017). Tumor cell death by pattern-sensing of exogenous RNA: Tumor cell TLR3 directly induces necroptosis by poly(I:C) in vivo, independent of immune effector-mediated tumor shrinkage. *Oncoimmunology* **6**, e1078968.

**Takeuchi, O. and Akira, S.** (2009). Innate immunity to virus infection. *Immunol Rev* **227**, 75-86.

**Unno, H., Futamura, K., Morita, H., Kojima, R., Arae, K., Nakae, S., Ida, H., Saito, H., Matsumoto, K. and Matsuda, A.** (2014). Silica and Double-Stranded RNA Synergistically Induce Bronchial Epithelial Apoptosis and Airway Inflammation. *American Journal of Respiratory Cell and Molecular Biology* **51**, 344-353.

**Van Opdenbosch, N. and Lamkanfi, M.** (2019). Caspases in Cell Death, Inflammation, and Disease. *Immunity* **50**, 1352-1364.

**Wang, L., Chang, X., Feng, J., Yu, J. and Chen, G.** (2019). TRADD Mediates RIPK1-Independent Necroptosis Induced by Tumor Necrosis Factor. *Front Cell Dev Biol* **7**, 393.

**Xia, P., Wang, S., Du, Y., Zhao, Z., Shi, L., Sun, L., Huang, G., Ye, B., Li, C., Dai, Z. et al.** (2013). WASH inhibits autophagy through suppression of Beclin 1 ubiquitination. *EMBO J* **32**, 2685-96.

**Yu, C. Y., Chiang, R. L., Chang, T. H., Liao, C. L. and Lin, Y. L.** (2010). The interferon stimulator mitochondrial antiviral signaling protein facilitates cell death by disrupting the mitochondrial membrane potential and by activating caspases. *J Virol* **84**, 2421-31.

**Yu, S. X., Zhou, F. H., Chen, W., Jiang, G. M., Du, C. T., Hu, G. Q., Liu, Z. Z., Yan, S. Q., Gu, J. M., Deng, X. M. et al.** (2017). Decidual Stromal Cell Necroptosis Contributes to Polyinosinic-Polycytidylic Acid-Triggered Abnormal Murine Pregnancy. *Front Immunol* **8**, 916.

**Zhang, P., Li, Y., Xia, J., He, J., Pu, J., Xie, J., Wu, S., Feng, L., Huang, X. and Zhang, P.** (2014). IPS-1 plays an essential role in dsRNA-induced stress granule formation by interacting with PKR and promoting its activation. *J Cell Sci* **127**, 2471-82.

**Zhao, X., Ai, M., Guo, Y., Zhou, X., Wang, L., Li, X. and Yao, C.** (2012). Poly I:C-induced tumor cell apoptosis mediated by pattern-recognition receptors. *Cancer Biother Radiopharm* **27**, 530-4.

**Zhou, X., You, F., Chen, H. and Jiang, Z.** (2012). Poly(C)-binding protein 1 (PCBP1) mediates housekeeping degradation of mitochondrial antiviral signaling (MAVS). *Cell Res* **22**, 717-27.

## Figures

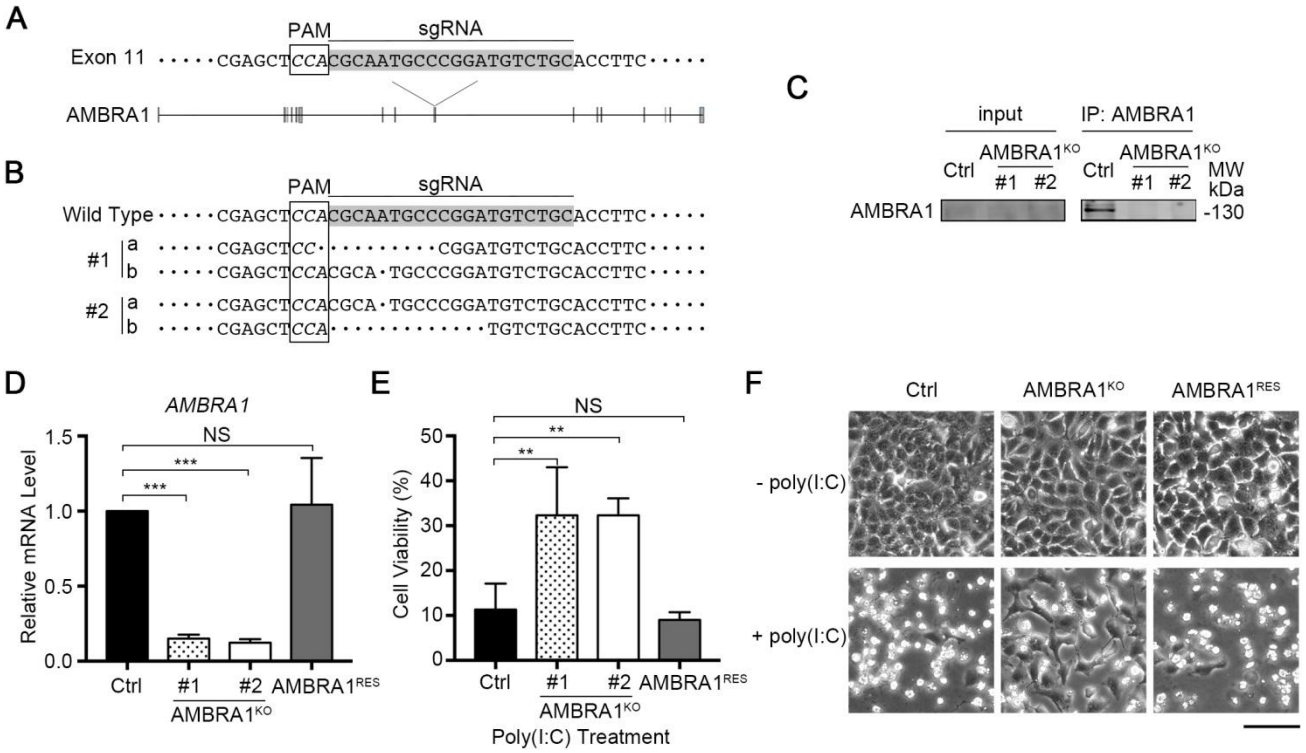


**Fig. 1. AMBRA1 promotes dsRNA-induced cell death.** (A) Sequence of sgRNA against CDS region of *AMBRA1* gene. (B) Sequences of two AMBRA1$^{KO}$ cell clones. Genomic DNA of two cell clones was extracted and then the region surrounding sgRNA targeting sequence was amplified and sequenced. (C) co-IP assay. The cell lysates of the control and two cell clones were incubated with anti-AMBRA1 antibody. The levels of AMBRA1 were detected by western blot. (D) qRT-PCR analysis of *AMBRA1* mRNA levels. Total RNAs of the control, AMBRA1$^{KO}$, and AMBRA1$^{RES}$ A549 cells were extracted for qRT-PCR analysis. Data were presented as mean ± standard deviation (SD) from three experiments; P values were calculated by ANOVA with Dunnett's multiple comparison test; ***p < 0.001 and NS, not significant. (E) Cell viabilities measured by MTT. The control, AMBRA1$^{KO}$, and AMBRA1$^{RES}$ A549 cells were transfected with 1 μg/ml poly(I:C). MTT assay was performed at 24 h post-transfection. Data were presented as mean ± SD from three experiments; P values were calculated by ANOVA with Dunnett's multiple comparison test; **p < 0.01 and NS, not significant. (F) Cell images. The control, AMBRA1$^{KO}$, and AMBRA1$^{RES}$ A549 cells were transfected with 1 μg/ml poly(I:C). Then cell images were taken at 24 h post-transfection. Representative images of three independent experiments were shown. Scale bar, 50 μm.

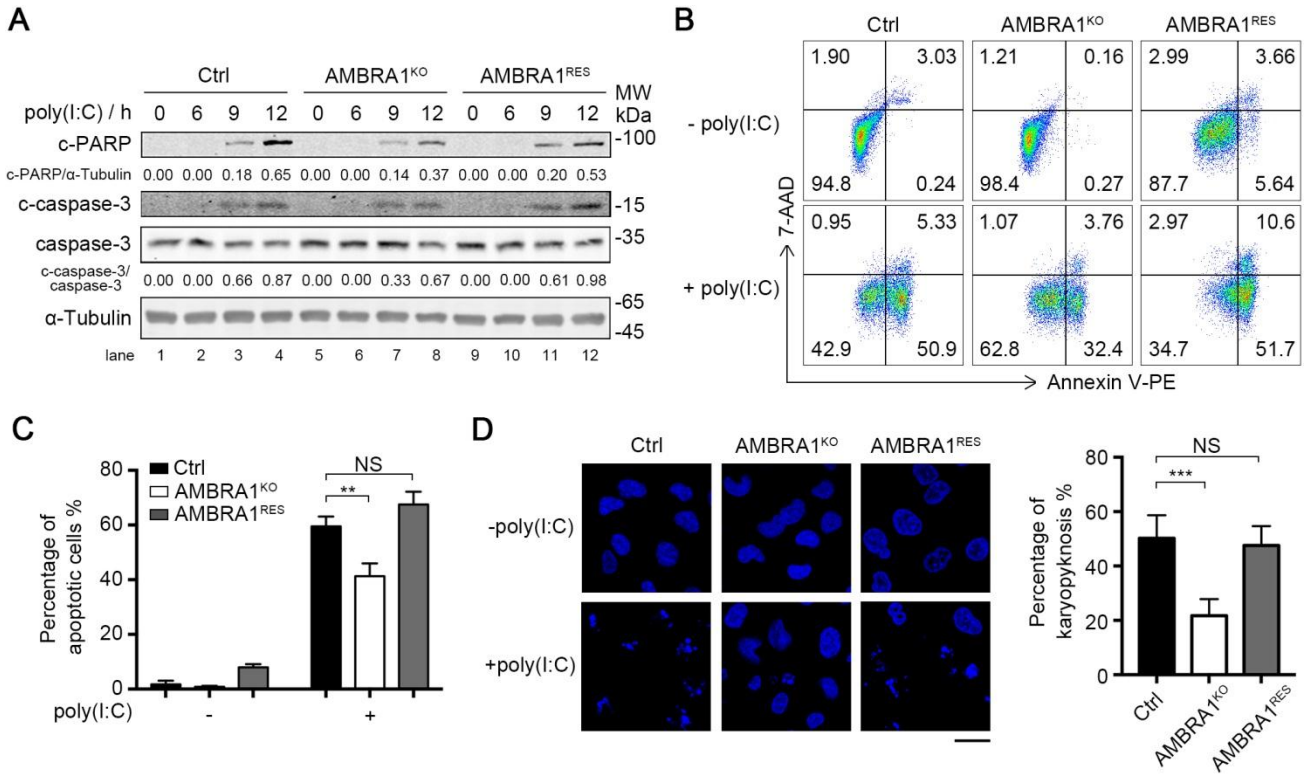


**Fig. 2. AMBRA1 is involved in the apoptosis induced by dsRNA.** (A) Western blot. The control, AMBRA1$^{KO}$, and AMBRA1$^{RES}$ A549 cells were transfected with 1 μg/ml poly(I:C) for indicated time. The cells were collected for measurement of caspase-3, c-caspase-3, and c-PARP by western blot. α-Tubulin was probed as an internal control. Representative blots of three independent experiments were presented. (B) Flow cytometry analysis. The control, AMBRA1$^{KO}$, and AMBRA1$^{RES}$ A549 cells were treated with 1 μg/ml poly(I:C) for 12 h. The whole cells were collected for flow cytometry analysis by staining with Annexin V-PE and 7-AAD (BD). Representative data of three independent experiments were shown. (C) Statistical analysis was carried out to reveal the proportion of apoptotic cells (Annexin V-PE -positive). Data were presented as mean ± SD from three experiments; P values were calculated by ANOVA with Dunnett's multiple comparison test; **p < 0.01 and NS, not significant. (D) Immunofluorescence microscopy. The control, AMBRA1$^{KO}$, and AMBRA1$^{RES}$ A549 cells were stimulated with 1 μg/ml poly(I:C). At 12 h post-transfection, the cells were stained with hoechst. Images were captured to reveal karyopyknosis. Representative images of three independent experiments were shown. Scale bar, 20 μm. P values were calculated by ANOVA with Dunnett's multiple comparison test; ***p < 0.001 and NS, not significant.

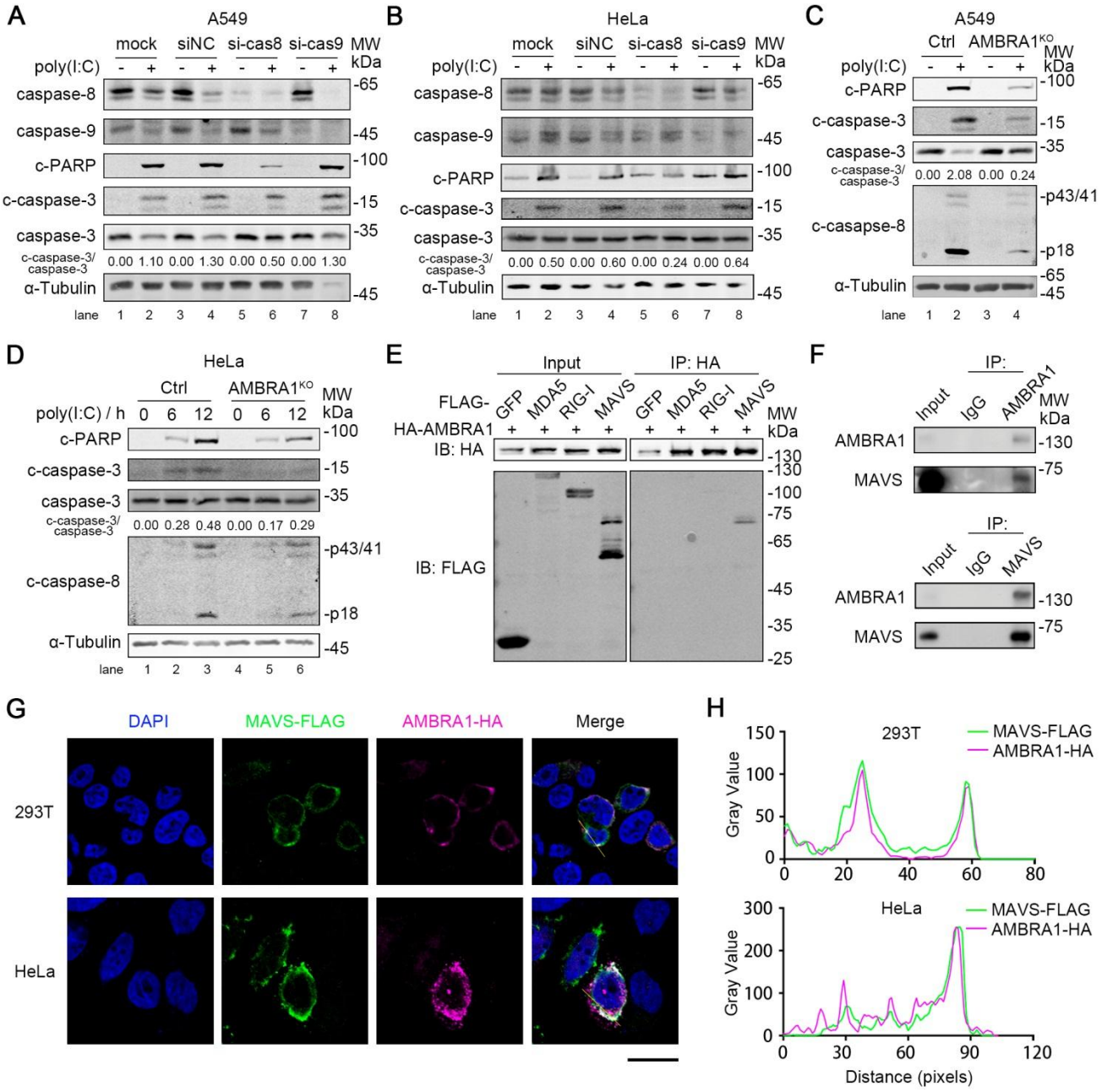


**Fig. 3. AMBRA1 interacts with MAVS.** (A, B) PARP and caspase-3 cleavage in A549 (A) and HeLa (B) cells. A549 or HeLa cells were transfected with siNC, si-caspase-8 (si-cas8), or si-caspase-9 (si-cas9). At 48 h post-transfection, A549 or HeLa cells were transfected with 1 μg/ml or 2 μg/ml poly(I:C) for 9 h respectively. Then, the whole cell lysates were harvested for the measurement of caspase-8, caspase-9, c-PARP, c-caspase-3, and caspase-3 levels. (C, D) C-PARP and c-caspase-8 levels. Control and AMBRA1$^{KO}$ A549 and HeLa cells were transfected with 1 μg/ml or 2 μg/ml poly(I:C), respectively. A549 cells were harvested at 12 h post-transfection (C), and HeLa cells were harvested at 6 h and 12 h post-transfection (D) for measurement of c-PARP, c-caspase-3,

caspase-3, and c-caspase-8 levels. (E) co-IP assay. 293T cells were co-transfected with plasmid expressing AMBRA1-HA with plasmids expressing FLAG-tagged GFP, MDA5, RIG-I, and MAVS. At 24 h post-transfection, the whole-cell lysates were harvested and then prepared for co-IP assay using anti-HA antibody. Western blot was performed to detect the interaction. IB: immunoblot. (F) Endogenous AMBRA1 and MAVS interaction in A549 cells. Cell lysates of A549 cells were collected for immunoprecipitation using anti-AMBRA1 antibody or anti-MAVS antibody. (G) Subcellular localization of AMBRA1 and MAVS. 293T and HeLa cells were co-transfected with plasmids expressing AMBRA1-HA and MAVS-FLAG. Anti-FLAG and anti-HA antibodies were used to indicate the subcellular localization of MAVS (green) and AMBRA1 (red). The nuclear was stained with DAPI (blue). Scale bar, 20 μm. (H) Colocalization analysis using Image J software was shown. α-Tubulin was probed as an internal control (A, B, C, D). Representative blots of three independent experiments were presented.

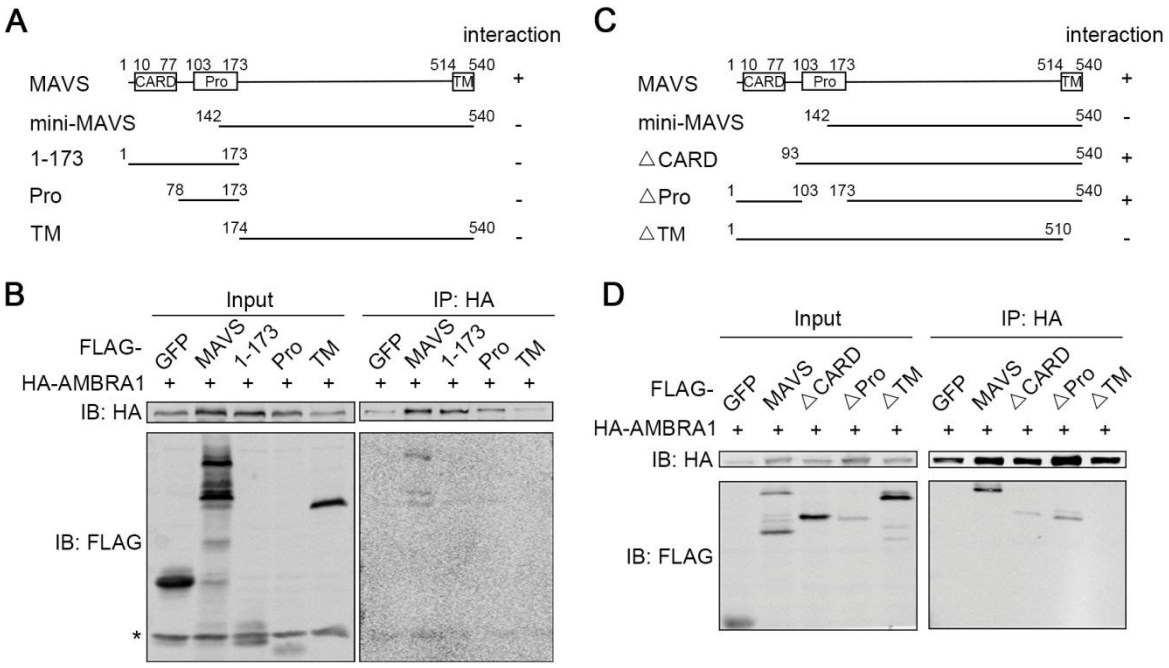


**Fig. 4. TM domain of MAVS is indispensable for MAVS to interact with AMBRA1**. (A, C) Schematic illustration of constructs expressing truncated MAVS. (B, D) Co-IP assay to map the AMBRA1-interacting domain of MAVS. 293T cells were co-transfected with plasmid expressing AMBRA1-HA with different truncates of MAVS. The cell lysates were harvested for co-IP assay using anti-HA antibody. Representative blots of at least three independent experiments were presented. Asterisk indicated nonspecific bands.

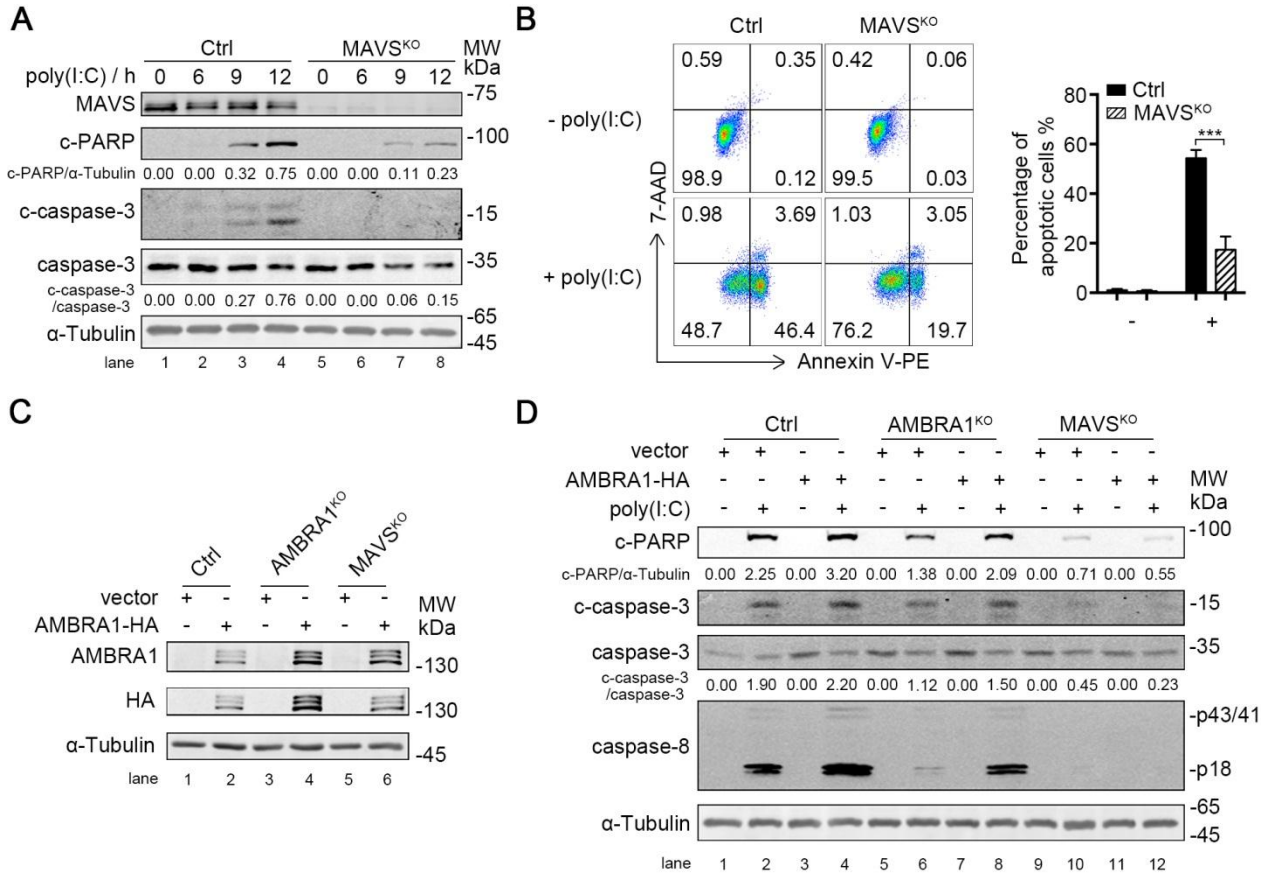


**Fig. 5. The pro-apoptotic role of AMBRA1 is dependent of MAVS.** (A) Caspase-3, c-caspase-3, and c-PARP measured by western blot. The control and MAVS$^{KO}$ A549 cells were transfected with 1 μg/ml poly(I:C). At indicated time points post-transfection, the cells were harvested for measurement of caspase-3, c-caspase-3, and c-PARP. The depletion of MAVS in MAVS$^{KO}$ A549 cells was also confirmed. (B) Flow cytometry analysis. The control and MAVS$^{KO}$ cells were transfected with 1 μg/ml poly(I:C). At 12 h post-transfection, the cells were collected for flow cytometry analysis by staining with Annexin V-PE and 7-AAD. Representative data of three independent experiments were shown. The statistical results of apoptosis (Annexin V-PE-positive) were shown. Data were presented as mean ± SD from three experiments; P value was calculated by unpaired, two-tailed student's t-test; ***$p < 0.001$. (C) Western blot. The control, AMBRA1$^{KO}$, and MAVS$^{KO}$ A549 cells were transduced with lentivirus expressing AMBRA1-HA, vector serving as a negative control, and selected using blasticidin. Selected cells were harvested for western blot to analyze the ectopic expression of AMBRA1. (D) Western blot. Cells were transfected with 1 μg/ml poly(I:C) for 9 h. The whole cell lysates were collected for western blot to measure c-PARP, c-caspase-3, caspase-3, and c-caspase-8. α-Tubulin was probed as an internal control (A, C, D). Representative blots of three independent experiments were presented.

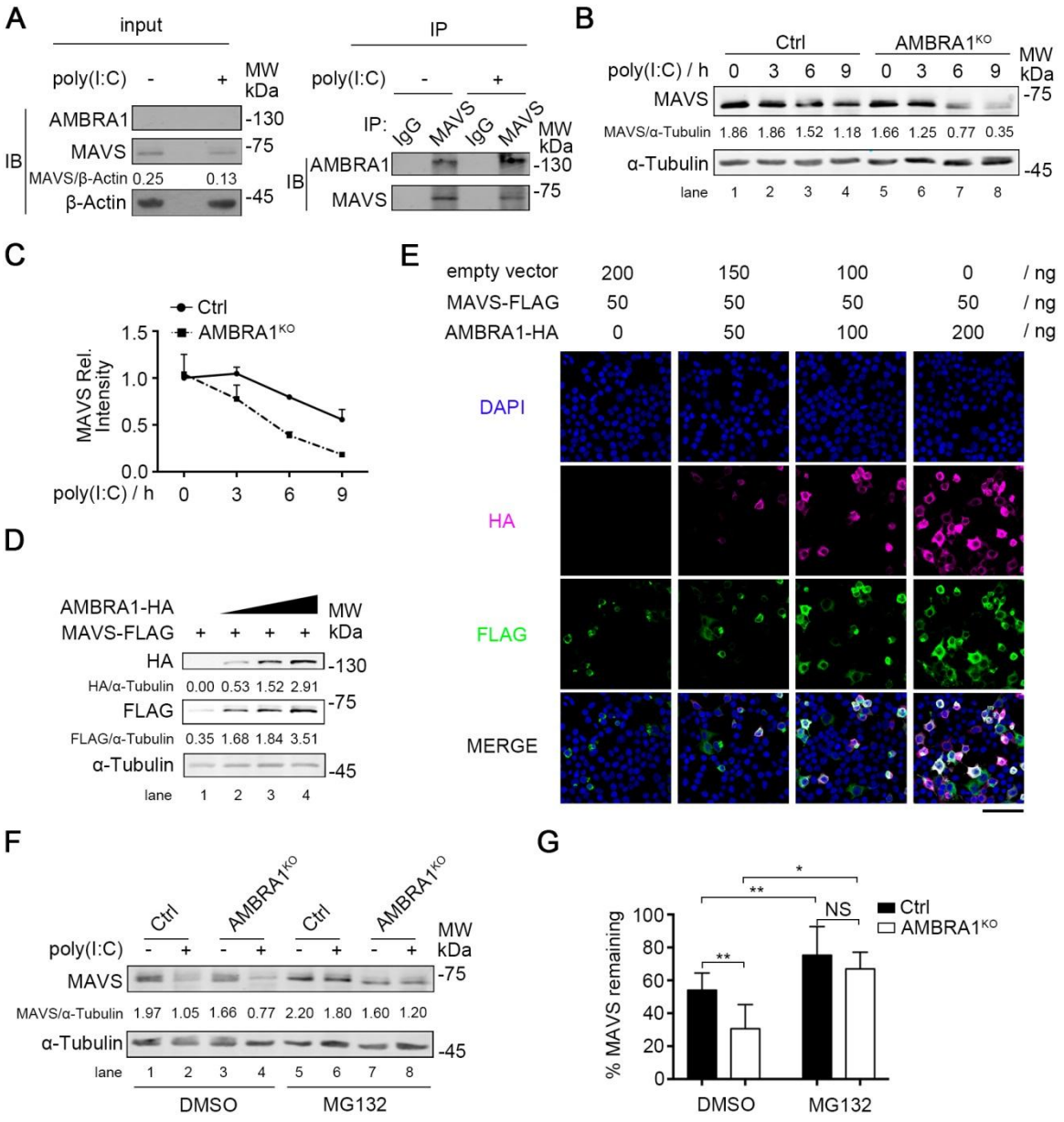


**Fig. 6. AMBRA1 maintains the stability of MAVS.** (A) Co-IP assay to detect the AMBRA1/ MAVS interaction. A549 cells were treated with 1 μg/ml poly(I:C) for 9 h, and the cell lysates were prepared for co-IP assay using anti-MAVS antibody. Western blot was performed to detect the interaction. Representative blots of three independent experiments were presented. β-Actin was probed as an internal control. (B) Western blot to measure the MAVS levels. The control and AMBRA1$^{KO}$ A549 cells were treated with 1 μg/ml poly(I:C) for indicated time. The protein levels of MAVS were measured by western blot, and α-Tubulin was probed as an internal control. Representative blots of three independent experiments were presented. (C) The relative intensities of MAVS were determined by normalizing the intensities of MAVS by the respective intensities of

α-Tubulin. (D) Western blot. 293T cells were co-transfected with 100 ng MAVS-FLAG with 0, 200, 400, or 800 ng AMBRA1-HA in 12-well plate. Empty vectors were used to fill up the whole dose of plasmids. Anti-FLAG and anti-HA antibodies were used to show the protein levels of MAVS-FLAG and AMBRA1-HA, and α-Tubulin was probed as an internal control. Representative blots of three independent experiments were presented. (E) Immunofluorescence assay. 293T cells were co-transfected with 50 ng MAVS-FLAG with 0, 50, 100, or 200 ng AMBRA1-HA in 24-well plate. Empty vectors were used to fill up the whole dose of plasmids. Anti-FLAG and anti-HA antibodies were used to indicate the subcellular localization of MAVS (green) and AMBRA1 (red). The nuclear was stained with DAPI (blue). Scale bar, 50 μm. (F) Western blot to measure the MAVS levels. The control and AMBRA1$^{KO}$ A549 cells were pretreated with 10 μM MG132, followed by treatment with 1 μg/ml poly(I:C). Transfected cells were harvested for western blot to detect MAVS protein at 9 h post-transfection, and α-Tubulin was probed as an internal control. Representative blots of three independent experiments were presented. (G) Statistical analysis was shown. Data were presented as mean ± SD from three experiments; P values were calculated by unpaired, two-tailed student's test; **$p < 0.01$, *$p < 0.05$ and NS, not significant.

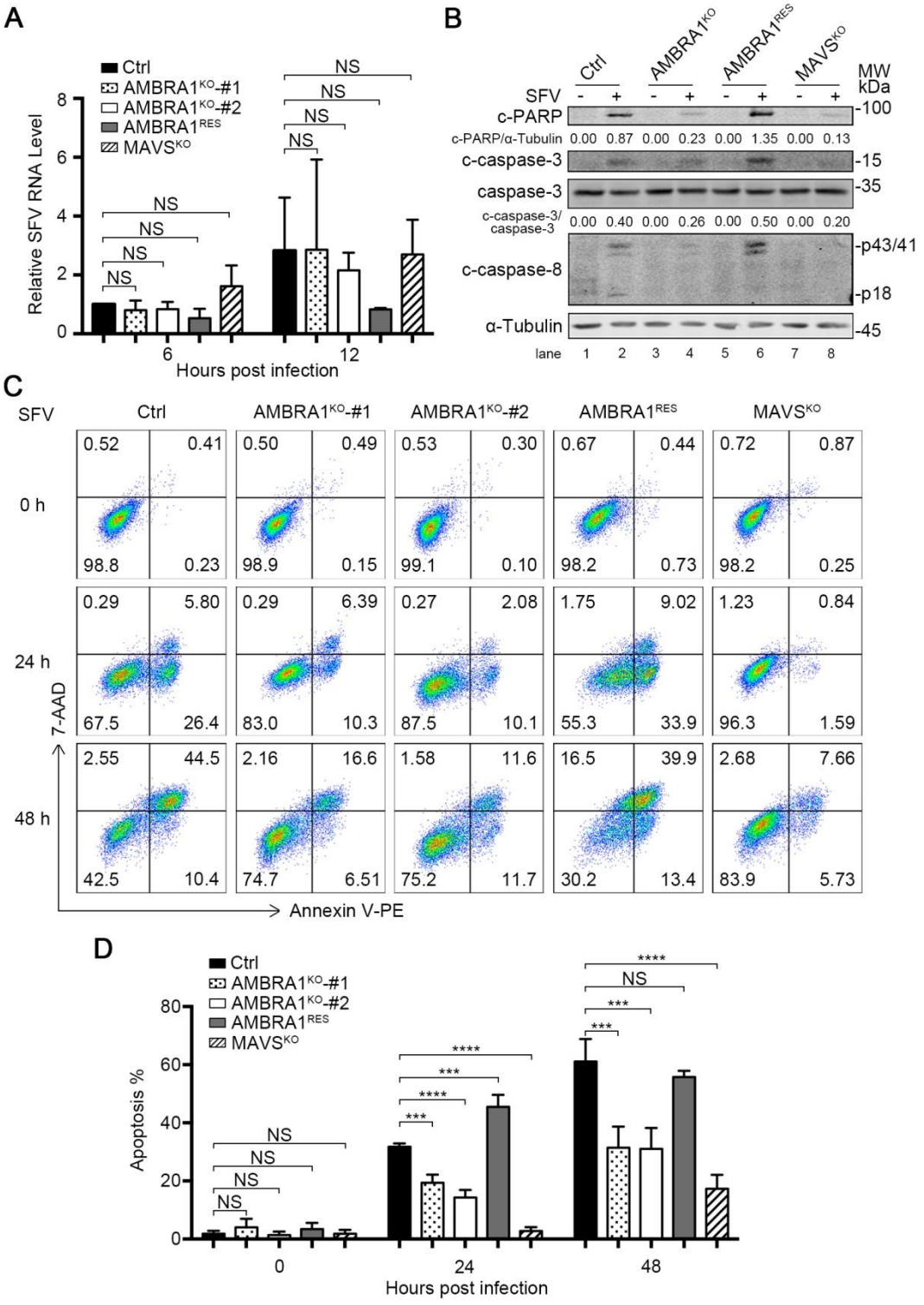


**Fig. 7. AMBRA1 promotes the apoptosis induced by SFV infection.** (A) SFV RNA levels. The control, AMBRA1$^{KO}$, AMBRA1$^{RES}$, and MAVS$^{KO}$ A549 cells were infected with SFV at an MOI of 1. At 6 h and 12 h post infection (h p.i.), the cells were harvested for qRT-PCR to determine the SFV RNA levels. Data were presented as mean ± SD from three experiments; P values were calculated by

ANOVA with Dunnett's multiple comparison test; NS, not significant. (B) C-PARP, caspase-3, c-caspase-3, and c-caspase-8 levels measured by western blot. The cells were infected with SFV at an MOI of 1. At 24 h p.i., the cells were collected for measurement of c-PARP, caspase-3, c-caspase-3, and c-caspase-8. α-Tubulin was probed as an internal control. Representative blots of three independent experiments were presented. (C) Flow cytometry analysis. The cells were infected with SFV at an MOI of 1 for 24 h and 48 h. Then the whole cells were collected for flow cytometry analysis by staining with Annexin V-PE and 7-AAD. Representative data of three independent experiments were shown. (D) Statistical analysis was carried out to reveal the proportion of apoptotic cells (Annexin V-PE-positive). Data were presented as mean ± SD from three experiments; P values were calculated by ANOVA with Dunnett's multiple comparison test; ***$p < 0.001$, ****$p < 0.0001$, and NS, not significant.

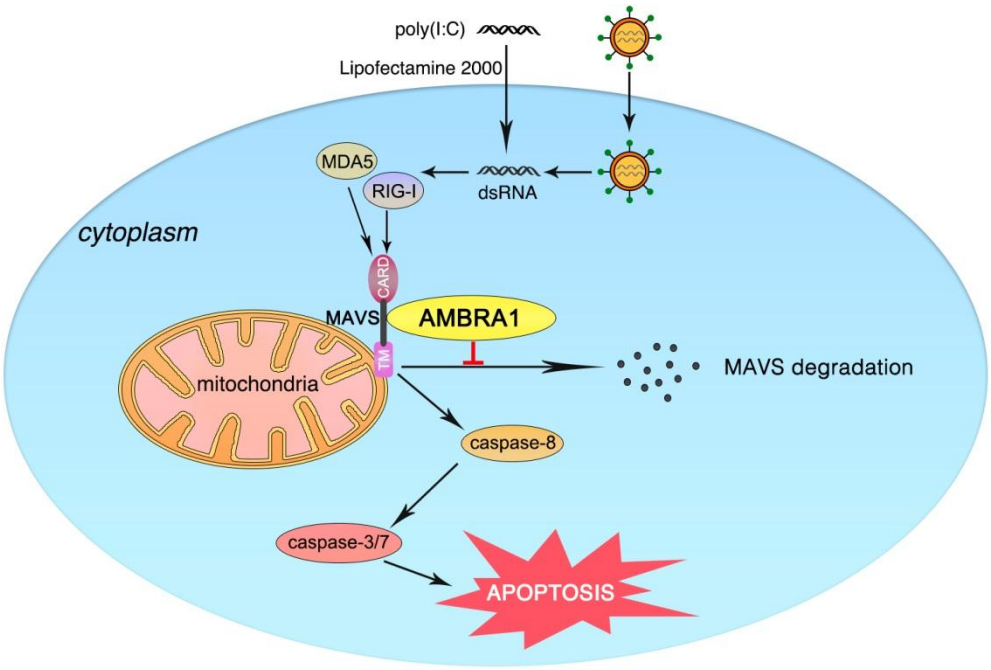


**Fig. 8. A proposed model to illustrate the mechanism by which AMBRA1 promotes apoptosis induced by dsRNA and virus.** In response to dsRNA or viral infection, MDA5 and/or RIG-I recognize dsRNA and signal to their adaptor, MAVS. MAVS recruits and activates the initiator caspase-8, and subsequently activates executor caspase-3/7, resulting in apoptosis. AMBRA1 interacts with and stabilizes MAVS through preventing the proteasomal degradation of MAVS, therefore promoting induction of apoptosis.

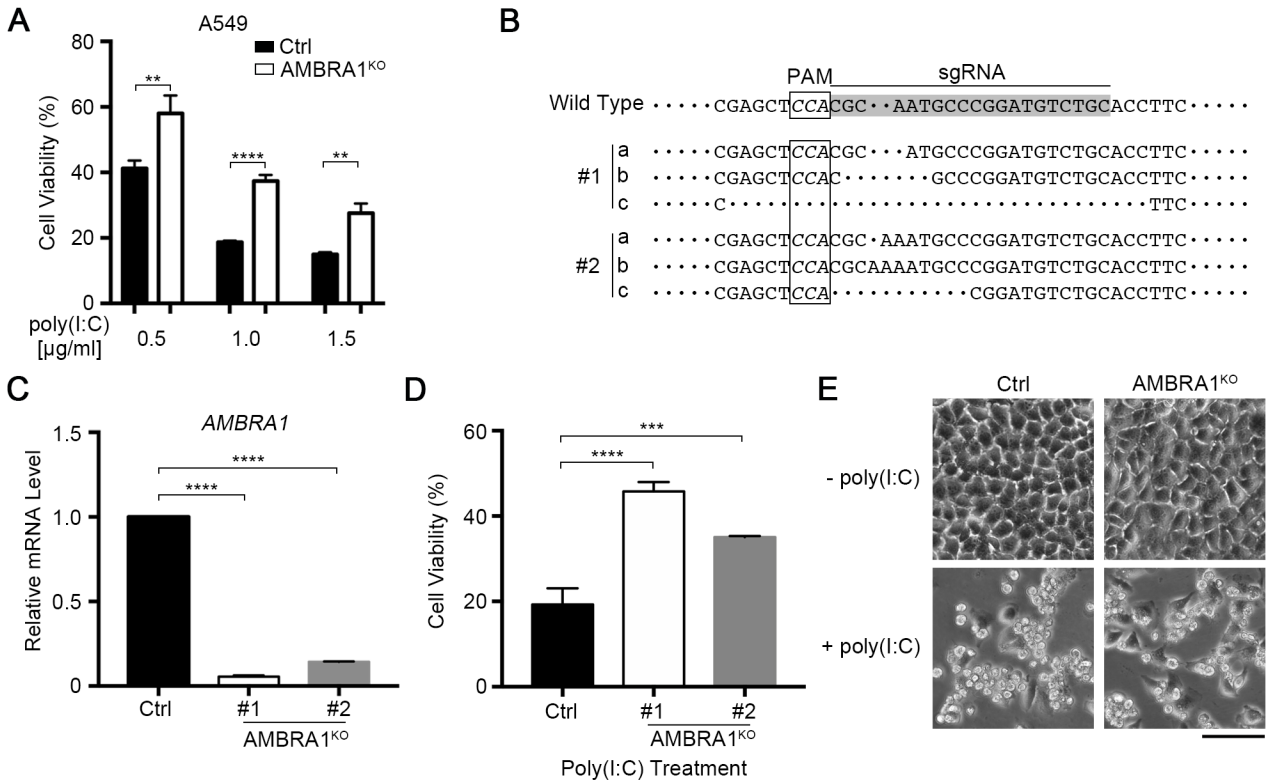


**Fig. S1. AMBRA1 promotes dsRNA-induced cell death.** (A) Cell viabilities. The control and AMBRA1$^{KO}$ cells were transfected with 0.5, 1, and 1.5 μg/ml poly(I:C). At 24 h post-transfection, cell viabilities were measured by CCK8 assay. P values were calculated by unpaired, two-tailed student's test; ****p < 0.0001, **p < 0.01. (B) Sequences of two HeLa AMBRA1$^{KO}$ cell clones. Genomic DNA was extracted and the region surrounding sgRNA targeting sequences was amplified and sequenced. (C) *AMBRA1* mRNA levels. Total RNAs of the control and two AMBRA1$^{KO}$ HeLa cell clones were extracted and applied for qRT-PCR. Data were presented as mean ± SD from three experiments; P values were calculated by ANOVA with Dunnett's multiple comparison test; ****p < 0.0001. (D) Cell viabilities. The control and two AMBRA1$^{KO}$ HeLa cell clones were transfected with poly(I:C). MTT assay was performed at 24 h post-transfection. Data were presented as mean ± SD from three experiments; P values were calculated by ANOVA with Dunnett's multiple comparison test; ***p < 0.001, ****p < 0.0001. (E) Cell images. The control and AMBRA1$^{KO}$ HeLa cells were transfected with poly(I:C) and then cell images were taken at 24 h post-transfection. Representative images of three independent experiments were shown. Scale bar, 50 μm.

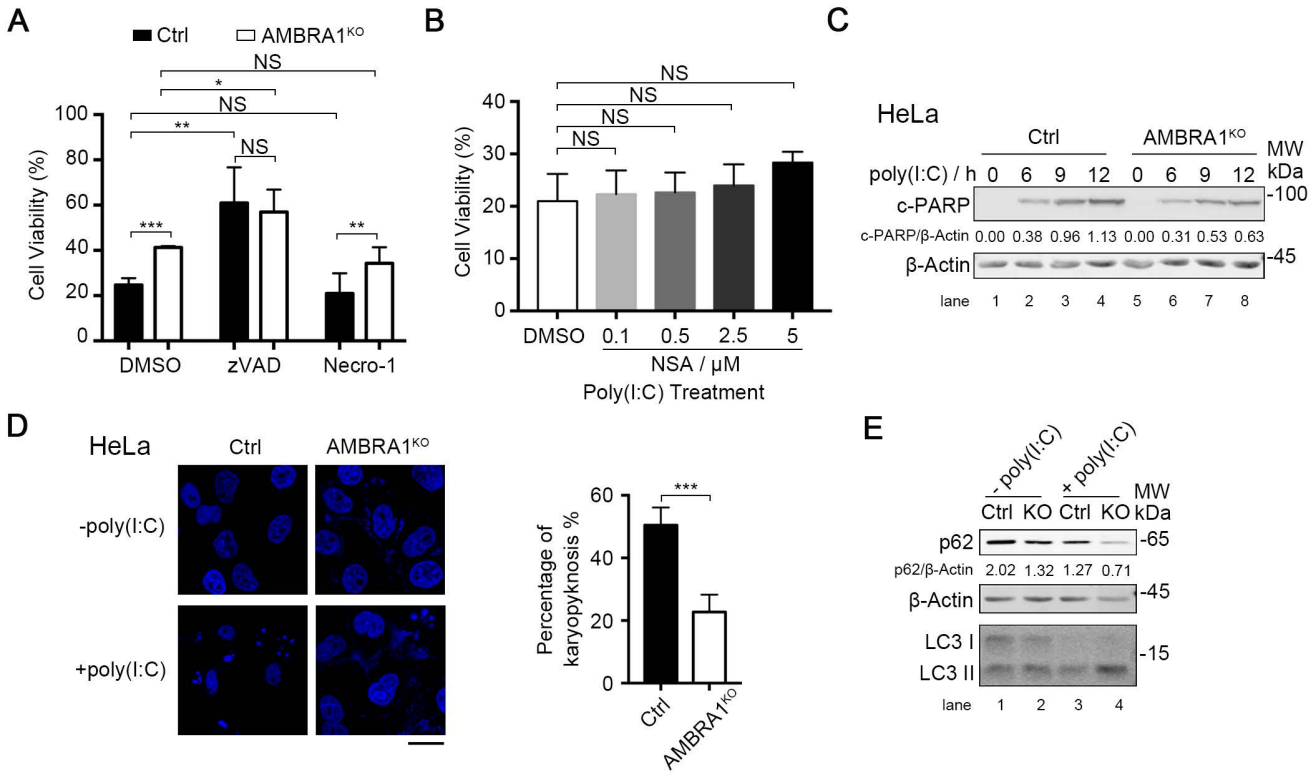


**Fig. S2. AMBRA1 promotes the dsRNA-induced apoptosis.** (A) Cell viability. The control and AMBRA1$^{KO}$ A549 cells were pretreated with DMSO, z-VAD(OMe)-FMK (zVAD) (50 μM) or Necrostatin-1 (Necro-1) (100 μM), followed by transfection with poly(I:C). The MTT assay was performed at 24 h post-transfection. Data were presented as mean ± SD from three experiments; P values were calculated by unpaired, two-tailed student's test; ***p < 0.001, **p < 0.01, and NS, not significant, or by ANOVA with Dunnett's multiple comparison test; **p < 0.01, *p < 0.05, and NS, not significant. (B) Cell viability. A549 cells were pretreated with DMSO or of Necrosulfonamide (NSA) at indicated concentrations for 1 h, followed by transfection with poly(I:C). The MTT assay was performed at 24 h post-transfection. Data were presented as mean ± SD from three experiments; P values were calculated by ANOVA with Dunnett's multiple comparison test; NS, not significant. (C) Western blot. The control and AMBRA1$^{KO}$ HeLa cells were treated with poly(I:C) for indicated time and then c-PARP was measured by western blot. α-Tubulin was probed as an internal control. Representative blots of three independent experiments were presented. (D) Immunofluorescence microscopy. The control and AMBRA1$^{KO}$ HeLa cells were transfected with poly(I:C) for 12 h and then stained with hoechst. Cell images were taken to reveal karyopyknosis. Representative images of three independent experiments were shown. Scale bar, 20 μm. P values were calculated by unpaired, two-tailed student's test; ***p < 0.001. (E) Western blot. The control and AMBRA1$^{KO}$ A549 cells

were stimulated with poly(I:C). At 9 h post-transfection, the whole cell lysates were collected for detection of p62 and LC3 I/II levels. β-actin was probed as an internal control. Representative blots of three independent experiments were presented.

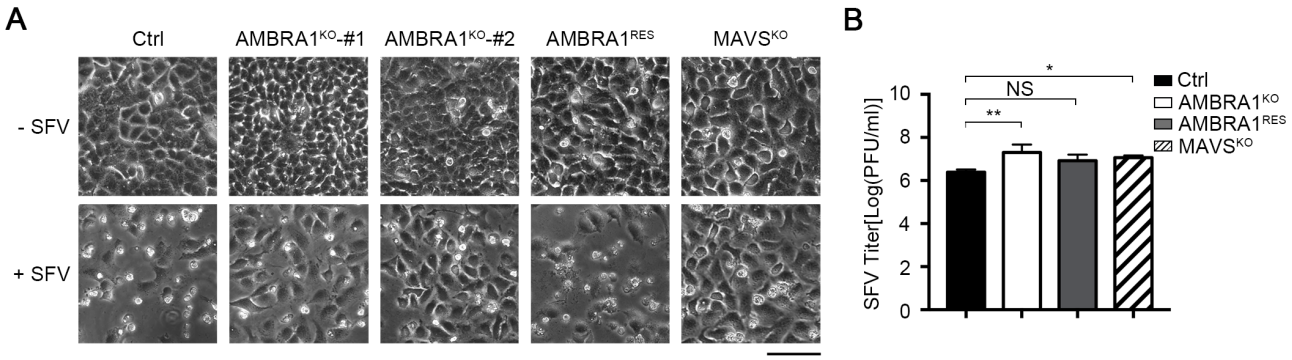


**Fig. S3. Effects of AMBRA1 or MAVS depletion on the cell death induced by SFV and viral replication.** (A) The control, AMBRA1$^{KO}$, AMBRA1$^{RES}$, and MAVS$^{KO}$ A549 cells were infected with SFV. Cell images were taken at 48 h p.i. Representative images of three independent experiments were shown. Scale bar, 50 μm. (B) Viral titers. The supernatants were collected at 24 h p.i. for plaque assay. Data were presented as mean ± SD from three experiments; P values were calculated by ANOVA with Dunnett's multiple comparison test; **p < 0.01, *p < 0.05, and NS, not significant.

**Table S1. Sequences of oligos used in CRISPR/Cas9 gene editing**

| Genes | Primers | Sequences (5'-3') | Targeting region |
|---|---|---|---|
| AMBRA1 | sg-AMBRA1-5F | GCAGACATCCGGGCATTGCG | Exon 11 |
| | sg-AMBRA1-3R | CGCAATGCCCGGATGTCTGC | |
| MAVS | sg-MAVS-5F | CTGTGAGCTAGTTGATCTCG | Exon 3 |
| | sg-MAVS-3R | CGAGATCAACTAGCTCACAG | |

**Table S2. Sequences of primers used in PCR amplification of gene fragments**

| Genes | Sequences (5'-3') |
|---|---|
| AMBRA1-5F | ATTTGCGGCCGCATGAAGGTTGTCCCAGAAAAGAATGC |
| AMBRA1-FLAG-3R | TTGCGGCCGCCTACTTATCGTCGTCATCCTTGTAATCACCA CCACCCCTGTTCCGTGGTTCTCCCCTAG |
| AMBRA1-NGG-5F | TGATAGATCAAGGCACCGAGCTGCACGTAAT |
| AMBRA1-NGG-3R | CAGACATTCGTGCATTACGTGCAGCTCG |
| AMBRA1-5F | CGGAATTCATGAAGGTTGTCCCAGAAAAGAATGC |
| AMBRA1-HA-3R | CCAAGCTTCTAAGCGTAATCTGGAACATCGTATGGGTAACC ACCACCCCTGTTCCGTGGTTCTCCCCTAG |
| AMBRA1-5F | CTCTAGATCGCGAACGCGTATGAAGGTAGTGCCTGAAAAG A |
| AMBRA1-HA-3R | GCCGCCCTCGAGGAATTCCTAAGCGTAATCTGGAACATCGT ATGGGTAACCACCACCCCTGTTCCGTGGTTCTCCCCTAG |
| MDA5-5F | CGGGATCCATGTCGAATGGGTATTCCACA |
| MDA5-FLAG-3R | CCGCTCGAGCTACTTATCGTCGTCATCCTTGTAATCACCAC CACCATCCTCATCACTAAATAAACAGC |
| RIG-I-5F | CCCAAGCTTATGACCACCGAGCAACGACG |
| RIG-I-FLAG-3R | CCGCTCGAGTCACTTATCGTCGTCATCCTTGTAATCACCAC CACCTTTGGACATTTCTGCTGG |
| 1-173-5F (MAVS) | CCAAGCTTATGCCGTTTGCTGAAGACAA |
| 1-173-FLAG-3R (MAVS) | CCCTCGAGCTACTTATCGTCGTCATCCTTGTAATCACCACC ACCTGGATTCCTTGGGATGGCTCT |
| AMBRA1-TA clone-5F | AAGACAACCCCCCAAGACACA |
| AMBRA1-TA clone-3R | TGGCTAACCATCATCCGTCAAGAG |

**Table S3. Sequences of primers used in qRT-PCR.**

| Genes | Sequences (5'-3') |
|---|---|
| *AMBRA1*-5F | AGCTCCACGCAATGCCCGGAT |
| *AMBRA1*-3R | CAGACTGTCCATCACCGATCACT |
| *β-actin*-5F | GCTCCTCCTGAGCGCAAG |
| *β-actin*-3R | CATCTGCTGGAAGGTGGACA |
| SFV-5F | CCGGAGGACGCACAGAAGTTG |
| SFV-3R | TGCGACGGCCACAATCGGAAG |